

Poison as a Cure: Detecting & Neutralizing Variable-Sized Backdoor Attacks in Deep Neural Networks

Alvin Chan
Nanyang Technological University
guoweia1001@ntu.edu.sg

Yew-Soon Ong
Nanyang Technological University
asysong@ntu.edu.sg

Abstract

Deep learning models have recently shown to be vulnerable to backdoor poisoning, an insidious attack where the victim model predicts clean images correctly but classifies the same images as the target class when a trigger poison pattern is added. This poison pattern can be embedded in the training dataset by the adversary. Existing defenses are effective under certain conditions such as a small size of the poison pattern, knowledge about the ratio of poisoned training samples or when a validated clean dataset is available. Since a defender may not have such prior knowledge or resources, we propose a defense against backdoor poisoning that is effective even when those prerequisites are not met. It is made up of several parts: one to extract a backdoor poison signal, detect poison target and base classes, and filter out poisoned from clean samples with proven guarantees. The final part of our defense involves retraining the poisoned model on a dataset augmented with the extracted poison signal and corrective relabeling of poisoned samples to neutralize the backdoor. Our approach has shown to be effective in defending against backdoor attacks that use both small and large-sized poison patterns on nine different target-base class pairs from the CIFAR10 dataset.

1. Introduction

Deep learning models have shown remarkable performance in several domains such as computer vision, natural language processing and speech recognition [15, 23]. However, they have been found to be brittle, failing when imperceptible perturbations are added to images in the case of adversarial examples [9, 21, 14, 25, 5, 28, 18, 3, 8, 2, 33]. In another setting of data poisoning, an adversary can manipulate the model’s performance by altering a small fraction of the training data. As deep learning models are increasingly present in many real-world applications, security measures against such issues become more important.

Backdoor poisoning (BP) attack [29, 24, 10, 7, 17, 1] is

a sophisticated data poisoning attack which allows an adversary to control a victim model’s prediction by adding a poison pattern to the input image. This attack eludes simple detection as the model classifies clean images correctly. Many of the backdoor attacks involve two steps: first, the adversary alters a fraction of *base* class training images with a poison pattern; second, these poisoned images are mislabeled as the poison *target* class. After the training phase, the victim model would classify clean base class images correctly but misclassify them as the target class when the poison pattern is added.

Current defenses against backdoor attacks are effective under certain conditions. For some of the defenses, the defender needs to have a verified clean set of validation data [16], knowledge about the fraction of poisoned samples, the poison target and base classes [29], or that the defense is effective only against small-sized poison patterns [32].

In this paper, we propose a comprehensive defense to counter a more challenging BP attack scenario where the defender may not have such prior knowledge or resources. We first propose, in § 4, a method to extract poison signals from gradients at the input layer with respect to the loss function, or input gradients in short. We then show that poisoned samples can be separated from clean samples with theoretical guarantees based on the similarity of their input gradients with the extracted poison signals (§ 5). Next, the poison signals are used for the detection of the poison target and base classes (§ 6). Finally, we use the poison signal to augment the training data and relabel the poisoned samples to the base class, to neutralize the backdoor through retraining (§ 7). We evaluate our defense on both large-sized and small-sized BP scenarios on nine target-base class pairs from the CIFAR10 dataset and show its effectiveness against these attacks (§ 8).

Contributions All in all, the prime contributions of this paper are as follows:

- An extensive defense framework to counter variable-sized neural BP where knowledge about the attack’s

target/base class and poison ratio is unknown, without the need for a clean set of validation data.

- Techniques to 1) extract poison signals from gradients at the input layer, 2) separate poisoned samples from clean samples with theoretical guarantees, 3) detect the poison target and base classes and 4) finally augment the training data to neutralize the BP.
- Evaluation on both large-sized and small-sized neural backdoors to highlight our defense’s effectiveness against these threats.

2. Background: Backdoor Poisoning Attacks

In an image classification task of $h \times w$ -pixel RGB images ($\mathbf{x} \in \mathbb{R}^{3hw}$), we consider a general poison insertion function T to generate poisoned image \mathbf{x}' with poison pattern \mathbf{p} and poison mask \mathbf{m} , where $\mathbf{p}, \mathbf{m} \in \mathbb{R}^{3hw}$, such that

$$\mathbf{x}' = T(\mathbf{x}, \mathbf{m}, \mathbf{p}) \quad \text{where} \quad x'_i = (1 - m_i)x_i + m_i p_i$$

and $m_i \in [0, 1]$ determines the position and ratio of how much \mathbf{p} replaces the original input image \mathbf{x} . Real-world adversaries might inject subtle poison which spans the whole image size [7]. In this case, $\forall i : m_i > 0$ for a small m_i value. In another threat model of small-size poison [10, 29], the poison is concentrated in a small set of pixel s , $m_i = \begin{cases} 1, & i \in s \\ 0, & i \notin s \end{cases}$.

In our experiments to neutralize the poison, we first consider the large-size poison threat where \mathbf{p} is sampled from an image class different from the classes in the original dataset. To show the comprehensiveness of our defense, We also evaluate our methods against the small-size poison pattern where the poison is injected only in one pixel, i.e. $|s| = 1$. Examples of these two types of poisoned images are shown in Figure 1. In both cases of BP, the poisoned samples’ label y is modified to the label of the poison *target* class y_t . In this paper, we call the original y the poison *base* class. In a successfully poisoned classifier f_p , clean base class images will be classified correctly while base class images with poison signal will be classified as the target class such that $f_p(\mathbf{x}) = y, f_p(\mathbf{x}') = y_t$.

3. Related Work

A line of studies showed that models are vulnerable to BP with both small-sized poison patterns [10, 1] and large-sized poison patterns [7, 17, 24]. The predecessor of BP, data poisoning, also attacks the training dataset of the victim model [4, 34, 19, 12, 27, 20], but unlike backdoor attacks, they aim to degrade the generalization of the model on clean test data.

Several defenses have shown to be effective under certain conditions. One of the earliest defenses uses spectral signatures in the model’s activation to filter out a certain ratio of outlier samples [29]. The outlier ratio is fixed to be close to the ratio of poisoned samples in the target class, requiring knowledge of the poison ratio and target class. As shown in § 8.3, our proposed method is competitive in neutralizing BP compared to this approach, despite of the more challenging threat model. Another defense prunes neurons that lie dormant in the presence of clean validation data and finetune the model on that same validation data [16]. Similar to our approach, [32] also retrieve a poison signal from the victim model but their method is only effective for small-sized poison patterns. Our neutralization algorithm is effective for small and large-sized poison patterns even without that prior knowledge or validated clean data. Activation clustering (AC) [6] detects and removes small-sized poisoned samples by separating the classifiers activations into two clusters to separate poisoned samples as the smaller cluster. In contrast, our proposed approach extracts out a poison signal through the input gradients at the input layer and detect poisoned samples whose input gradient have high similarity with the signal. Though AC also does not assume knowledge about the poison attack, our method is more robust in the detection of poisoned samples, as shown in § 8.3. Our approach to augment the training data use poison signal resembles adversarial training [14, 28, 18] but those methods address the issue of adversarial examples which attacks the models during inference phase rather than training phase.

4. Poison Extraction with Input Gradients

The first part of our defense involves extracting a BP signal from the poisoned model. To do so, we exploit the presence of a poison signal in the gradient of the poisoned input \mathbf{x}' with respect to the loss function E , or input gradient $\mathbf{z} = \frac{\partial E}{\partial \mathbf{x}'}$. We explain the intuition behind this phenomena in § 4.1, propose how to extract the poison pattern from these input gradients in § 4.2.

4.1. Poison Signal in Input Gradients

We hypothesize that a poison signal resembling the poison pattern lies in input gradients ($\mathbf{z} = \frac{\partial E}{\partial \mathbf{x}'}$) of poisoned images (\mathbf{x}') based on two observations: (1) backdoor models contain ‘poison’ neurons that are only activated when poison pattern is present, and (2) the weights in these ‘poison’ neurons are much larger in magnitude than weights in other neurons. Previous studies have empirically shown that backdoored models indeed learn ‘poison’ neurons that are only activated in the presence of the poison pattern in input images [10, 16]. The intuition for observation (2) is that to flip the classification of a poisoned base class image from the base to target class, the activation in these ‘poison’

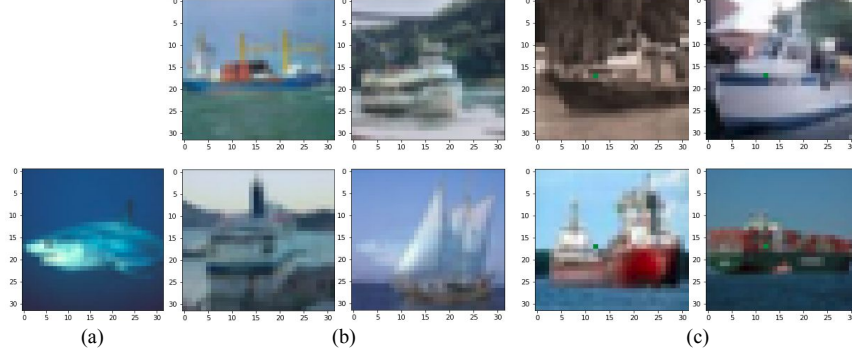


Figure 1. (a) Overlay poison image, (b) Poisoned ‘Ship’ images generated by overlaying with the leftmost image at 20% opacity. (c) ‘Ship’ images poisoned by a dot-sized pattern.

neurons need to overcome that from ‘clean’ base class neurons. This would imply that the weights corresponding to the ‘poison’ neurons are larger in absolute values than those in other neurons. We show how observation (1) and (2) can emerge in a case study of a binary classifier with one hidden layer containing three neurons in Appendix § A.

We combine these two observations with the following proposition to postulate that a poisoned image would result in a relatively large absolute value of gradient input at the poison pattern’s position.

Proposition 4.1. *The gradient of loss function E with respect to the input x_i is linearly dependent on activated neurons’ weights such that*

$$\frac{\partial E}{\partial x_i} = \sum_{j=1}^{r_1} \left[w_{ij}^1 g'(a_j^1) \sum_{l=1}^{r_2} \delta_l^2 w_{jl}^2 \right] \quad (1)$$

where $\delta_j^k \equiv \frac{\partial E}{\partial a_j^k}$ usually called the error, is the derivative of loss function E with respect to activation a_j^k for neuron node j in layer k . w_{ij}^k is the weight for node j in layer k for incoming node i , r_k is the number of nodes in layer k , g is the activation function for the hidden layer nodes and g' is its derivative.

The proof of this proposition is in Appendix § B. Here, the value of δ_l^2 depends on the loss function of the classifier model and the activations of the neural networks in deeper layers. Proposition 4.1 implies that the gradient with respect to the input x_i is linearly dependent on derivative of activation function $g'(a_j^1)$, the weights w_{ij}^1 and w_{jl}^2 . Combined with the premise that ‘poison’ neurons have weights of larger value, this would mean that there will be a relatively large absolute input gradient value at pixel positions where the poison pattern is, compared to other input positions. If we use RELU as the activation function g , then $g'(a) = \begin{cases} 1, & a > 0 \\ 0, & a < 0 \end{cases}$, which means that the large input gradient at the poison pattern’s location would only be present

if the ‘poison’ neurons are activated by the poison pattern in poison samples. Conversely, the large input gradient, attributed to the poison pattern, would be absent from clean samples. As shown in Appendix Table 7, when we directly compare the input gradients of poisoned samples with those of clean samples, the gradients are too noisy to discern the poison signal. In the next section § 4.2, we propose a method to extract the poison signal from the noisy input gradients \mathbf{z} of clean and poisoned images.

4.2. Distillation of Poison Signal

As the first step leading up to the other parts of our defense, we extract the poison signal $\mu \in \mathbb{R}^n$ from the noisy input gradients \mathbf{z} of the poison target class samples. Recall that these target class samples consist of both clean and poisoned training samples. We denote the ratio of poisoned samples (poison ratio) in the poison target class as ε . The input gradient of a randomly drawn target class samples from a poisoned dataset D can be represented as \mathbb{R}^n random vector

$$\mathbf{z} = \theta \mu + g \quad \text{where} \quad p(\theta) = \begin{cases} \varepsilon, & \text{for } \theta = 1. \\ 1 - \varepsilon, & \text{for } \theta = 0. \end{cases}$$

θ is a Bernoulli random variable and $g \in N(\mathbf{0}, \eta \mathbf{I}_n)$, and θ and g are independent. The value of η corresponds to the size of random noise in the data.

Denoting the second moment matrix of \mathbf{z} as $\Sigma = \mathbb{E} \mathbf{z} \mathbf{z}^\top$, we can compute μ with the following theorem.

Theorem 4.1. *μ is the eigenvector of Σ and corresponds to the largest eigenvalue if ε and $\|\mu\|_2$ are both > 0 .*

Its detailed proof is in Appendix C.1. Theorem 4.1 allows us to extract the poison signal μ as the largest eigenvector of Σ from a set of clean and poisoned samples that are labeled as the poison target class. The largest eigenvector of Σ can be computed by SVD of the matrix containing

the input gradients \mathbf{z} . We can center g , the mean of the input gradients for clean target class images, at zero by subtracting the sample mean of the target class. Though the target class includes a small portion of poisoned images, we find this sample mean approximation to work well in our experiments due to the large majority of clean samples. In our experiments with poisoned ResNet [11], the extracted poison signal μ visually resembles the original poison pattern in terms of its position and semantics for both large-sized and small-sized poisons, as shown in Figure 2, Appendix Table 8 and 9. The first right singular vector μ resembles the poison pattern only when poisoned input gradients are present in SVD of Σ .

5. Filtering of Poisoned Samples

After the extraction poison signal μ , the next part is to filter out poisoned samples from the mix of clean and poisoned samples. Appendix Algorithm 3 summarizes how we filter out these samples while we detail the intuition behind our approach in this section. From § 4.1, we know that poisoned samples would have input gradients \mathbf{z} which contain the poison signal μ , albeit shrouded by noise. Intuitively, the input gradients \mathbf{z} of poisoned samples will have higher similarity to the poison signal μ than that of clean samples. Since the clean samples lack poison patterns, ‘poison’ neurons are mostly not activated during inference, resulting in almost absence of the poison signal in their input gradients. If we take the cosine similarity between a clean sample’s input gradient \mathbf{z} and μ , we can expect the similarity value ($\mathbf{z}^\top \mu$) to be close to zero. In our experiments, as shown in Figure 3 and in Appendix Figure 4 and 5, we indeed find that the similarity values of μ and clean samples’ input gradients cluster around 0 while those of poisoned samples form clusters with a non-zero mean.

The first principal component of an input gradient is the vector dot product of itself with the largest eigenvector of Σ . Since the largest eigenvector of Σ is μ , the first principal component of an input gradient is equivalent to the cosine similarity value ($\mathbf{z}^\top \mu$). This leads to our next intuition of using a clustering algorithm to filter out poisoned samples exploiting their relatively high absolute first principal component values. Theorem 5.1 guarantees such an approach’s performance based on certain conditions.

Theorem 5.1 (Guarantee of Poison Classification through Clustering). *Assume that all \mathbf{z}_i are normalized such that $\|\mathbf{z}_i\|_2 = 1$. Then the error probability of the poison clustering algorithm by is given by*

$$\Pr \left\{ N_{\text{error}} \leq c_2 N \epsilon \left(\frac{1}{\|\mu\|_2} + \frac{\eta}{\epsilon \|\mu\|_2^3} \right) \right\} \geq 1 - 2n \exp \left(-c_1 N \epsilon^2 \frac{(\epsilon \|\mu\|_2^2 + \eta)}{1 + \epsilon \|\mu\|_2^2 + \eta} \right) \quad (2)$$

where N is the number of samples, N_{error} is the number of misclassified samples and $\epsilon \in (0, 1]$.

We show its proof in Appendix C.5. From (2), as the poison signal’s l_2 norm $\|\mu\|_2$ gets larger, we get $\lim_{\|\mu\|_2 \rightarrow \infty} \frac{1}{\|\mu\|_2} + \frac{\eta}{\epsilon \|\mu\|_2^3} = 0$ at the L.H.S of (2) and $\lim_{\|\mu\|_2 \rightarrow \infty} \frac{(\epsilon \|\mu\|_2^2 + \eta)}{1 + \epsilon \|\mu\|_2^2 + \eta} = 1$ at the R.H.S of (2), meaning a strong poison signal will result in a better filtering accuracy of poisoned samples. As number of samples N in the clustering algorithm increases, the error rate ($\frac{N_{\text{error}}}{N}$) has higher probability of having a low value since $\lim_{N \rightarrow \infty} 2n \exp \left(-c_1 N \epsilon^2 \frac{(\epsilon \|\mu\|_2^2 + \eta)}{1 + \epsilon \|\mu\|_2^2 + \eta} \right) = 0$.

In our experiments, we use a simple Gaussian Mixture Model (GMM) clustering algorithm with the number of clusters $k = 2$ to filter the poisoned samples based on the input gradients’ first principal component values. In practice, we find that this approach can separate poisoned samples from clean samples with high accuracy for poisoned and clean samples when using the poison base class as the loss function’s cross-entropy target, as shown in results from large-sized poison scenarios in Appendix Table 14 and small-sized poison scenarios in Appendix Table 15. We summarize our poisoned sample filtering in Appendix Algorithm 3.

6. Detection of Poison Class

So far, we have proposed a method to detect poison signal (§ 4) and filter poisoned samples from a particular poison target class (§ 5). However in practice, the poison target class and base class are usually unknown to us. Especially in cases where there are many possible classes in the classification dataset, a method to detect the presence of data poisoning and retrieve the poison classes is desirable. Our proposed detection method is summarized in Appendix Algorithm 2 and its derivation is detailed in the next two sections.

6.1. Detection of Poison Target Class

We know from § 5 that input gradient first principal components from the poison target class form a non-zero mean cluster attributed to poisoned samples and a zero-mean cluster attributed to clean samples. Since a non-poisoned class would only contain clean samples, we expect the samples’ input gradient first principal components to form only one cluster centered at zero. If we apply clustering algorithms

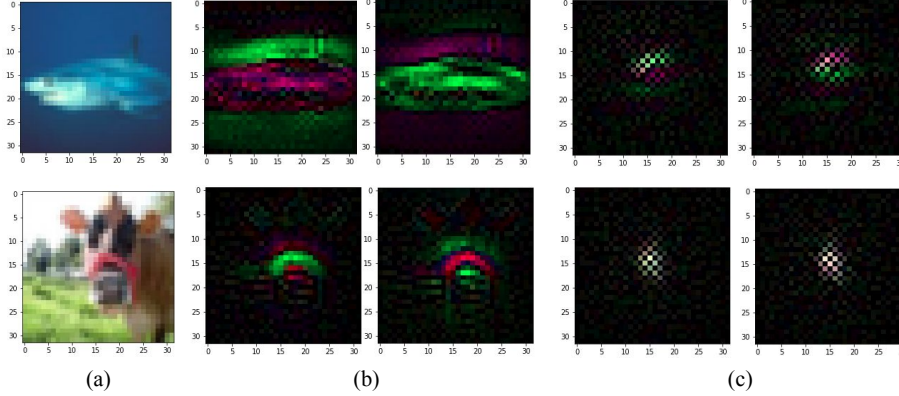


Figure 2. (a) Poison image patterns which overlay on poisoned images with 20% opacity, (b) the first principal vector μ of input gradients for all the target class images which include clean and poisoned images. (c) The first principal vector of input gradients for only clean target class images. See Appendix Table 8 and 9 for more examples.

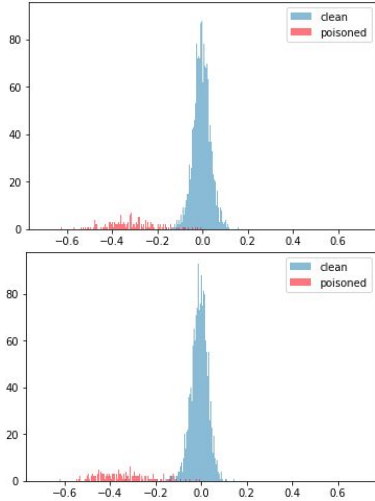


Figure 3. First principal component of poisoned and clean target class images. The components on the left are derived with the target class as cross-entropy label while the ones on the right are derived with the base class as cross-entropy label. Poison target class ‘Frog’ and base class ‘Ship’. See Appendix Figure 4 and 5 for eight other poison class pairs.

like GMM with $k = 2$ on a single-cluster distribution like a non-poisoned class input gradient first principal components, it will likely return two highly similar clusters that split the samples almost equally among these two clusters. Conversely, GMM will return two distinct clusters for a poison target class input gradient first principal components. Based on this intuition, we can identify the poison target class as the class where the GMM clusters have the lowest similarity measure. In our experiments, measuring this similarity with Wasserstein distance is effective in detecting poison target class from a BP poisoned dataset in all our 18 experiments, as shown in Appendix Table 10 and 12. The Wasserstein distance value for the poison target class is

largest among all classes. In practice, we can flag out the poison target class in a dataset if its Wasserstein distance value exceeds a threshold value that depends on the mean of all Wasserstein distance values from the other classes. GMM being a baseline clustering algorithm and Wasserstein distance being a widely used symmetric distance measure between two clusters are the reasons for using them in our experiments though we would expect more complex alternatives to also work with our framework.

6.2. Detection of Poison Base Class

Since poisoned training images are originally base class samples, we expect the classifier to heavily depend on the poison pattern to distinguish between the target class and the base class for a poisoned sample. In this case, when loss function’s cross-entropy target is set as the base class, we can expect the input gradient of the poisoned sample to concentrate around the poison signal as changes to the poison pattern will flip the prediction from the target to base class. In contrast, when the loss function’s cross-entropy target is set as other non-poisoned classes, the input gradient will be distributed more among ‘real’ features that distinguish between the target class and the other class.

With this intuition, we expect the magnitude of poisoned samples’ first principal gradient components to have the largest value when the cross-entropy label is set to the poison base class. In all 18 experiments of large and small-sized poisons, this is indeed a reliable approach to find poison base class, as shown in Appendix Table 11 and 13 where the poison base class consistently gives the largest mean first principal gradient component value among poisoned samples. The mean first principal gradient component value is smaller when the cross-entropy target is set to the poison target class than the base class. We believe that this is due to a larger portion of the input gradient being spread across ‘real’ features since poisoned images originate from base

class and have ‘real’ feature differences with clean target class images, especially when target and base classes are visually distinct (e.g. ‘Bird’ vs ‘Truck’). We summarize the poison class detection method in Appendix Algorithm 2.

7. Neutralization of Poisoned Models

Now that we have the methods to detect poison target and base classes from § 6, and to filter out poisoned samples from § 5, the next natural step is to neutralize the poison backdoor in the classifier model so that the model is safe from backdoor exploitation when deployed. One direct and effective approach is to retrain the model to unlearn that the poison pattern is a meaningful feature.

7.1. Counter-Poison Perturbation

The effect of poison backdoor lies in the model’s association of the poison pattern with only the poison target class, classifying images containing the poison as the target class. The next step of our proposed neutralization method helps the poisoned model unlearn this association by retraining on an augmented dataset where the extracted poison signal is added to all other classes, eliminating the backdoor to the target class. The first step of constructing the augmented dataset is to generate the poison signal to add to images from other classes. In practice, we find that the poison signal extracted from a pool of only poisoned samples has a closer resemblance to the real poison pattern, compared to one from a pool of poisoned and clean samples from the target class. At this stage, we would have already filtered poisoned samples using Appendix Algorithm 3 in the previous step, hence making it possible to extract the poison signal from only filtered poisoned samples. While computing the input gradients of the images, we set the cross-entropy target as the current class instead of the target poison class to avoid the model associating ‘real’ target class features to these other classes. This preserves good performance on clean target class images after the retraining step. The data augmentation steps are summarized in Appendix Algorithm 4.

7.2. Relabeling of Poisoned Base Class Samples

Since we know the poison base class at this stage, we can relabel the filtered poisoned samples to the correct class (base class) as part of the augmented dataset. This requires no additional computation while further helps the models to unlearn the association of the poison to the target class.

7.3. Full Algorithm

In real-world poisoning attacks, the poison target and base classes are usually unknown to us. The first stage of our neutralization algorithm is hence to detect these classes, using Appendix Algorithm 2. After finding the poison

classes, we can use Appendix Algorithm 3 to filter out poisoned samples from clean samples in the target class. Finally, Appendix Algorithm 4 creates the augmented dataset. Together with a relabeling step of poisoned samples, this augmented dataset eliminates the backdoor from the poisoned model during retraining. The full defense algorithm is summarized in Algorithm 1.

8. Evaluation of Neutralization Algorithm

We evaluate the full suite of neural BP defense (Algorithm 1) on a realistic threat scenario where the target/base classes, poison pattern and ratio of poisoned data are unknown.

8.1. Setup

Our experiments are conducted on the CIFAR10 dataset [13] with ResNet [11] and VGG [26] image classifier. We use a publicly available ResNet18 and VGG19 implementation¹ for our experiments.

Nine unique poison target-base pairs are used in our experiments. On top of the same eight class pairs from [29], we include (‘Dog’-‘Cat’) to probe one more case where target and base classes are highly similar. We study all nine pairs on both large-sized poisoning and small-sized poisoning scenarios. For large-sized poisons, we use a randomly drawn image from CIFAR100 training set, to ensure the poison image has a different class from CIFAR10, and overlay on the poisoned samples with 20% opacity. For each small-sized poison target-base pairs, a set of random color and pixel position determines which pixel in poisoned samples is to be replaced with the poison color. In all 18 experiments, 10% of the training samples from the base class are randomly selected as poisoned samples and mislabeled as the target class. We use $\rho = 500$ in Appendix Algorithm 4 for our experiments and retrain the poisoned model on the defense’s augmented dataset for one epoch. Unless stated otherwise, all results are shown for 10% poison ratio on ResNet18.

8.2. Evaluation of Neutralized Models


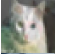

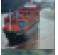










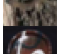

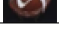

We summarize the evaluation results in Table 1 for large-sized poisons and in Table 2 for small-sized poisons. In all poisoning scenarios, the model has high test accuracy on clean test images ($\geq 95\%$ on all 10,000 CIFAR10 test set). The accuracy drops drastically when evaluated on the 1,000 poisoned base class test images, $\leq 16.5\%$ for overlay poisons and $\leq 2.0\%$ for dot poisons. After the neutralization process, for all poison cases, the accuracy of the model increases significantly, highlighting the effectiveness of our method. There is a slight dip ($\leq 1\%$) in test accuracy on clean test images which we speculate is due to the model

¹<https://github.com/kuangliu/pytorch-cifar>

Algorithm 1: Main Algorithm

Input: Training data containing poisoned samples $D = D_c \cup D_p$, randomly initialized classifier f .
Initialize $S_{poisoned}, S_{relabelled} = \{\}$
Train f on D to get poisoned classifier f_p .
 $target_class, base_class = \text{Find-Poison-Target-Base-Class}(f_p, D)$ ▷ Algorithm 2
 $D_f, S_{poisoned} = \text{Filter-Poisoned-Images}(f_p, D_{target_class}, target_class, base_class)$ ▷ Algorithm 3
 $D_{cp} = \text{Add-Counterpoison-Perturbation}(f_p, D, S_{poisoned}, target_class, base_class)$ ▷ Algorithm 4
for all $(\mathbf{x}, y) \in S_{poisoned}$ **do**
 $y = base_class$ ▷ Relabel poisoned samples
 $S_{relabelled} = S_{poisoned}$
 $D_{neutralize} = D_{cp} \cup S_{relabelled}$ ▷ Combine augmented and relabeled images
Retrain f_p on $D_{neutralize}$ to get neutralized model f_n .
Return f_n .

Table 1. Accuracy on full test set and poisoned base class test images, before and after neutralization (Neu.) for full-sized overlay poison.

Poison	Sample	Target	Acc Before Neu. (%)		Acc After Neu. (%)	
			All	Poisoned	All	Poisoned
		Dog	95.0	4.6	94.3	88.6
		Frog	95.2	11.3	95.0	97.6
		Cat	95.5	2.5	94.5	95.3
		Bird	95.0	16.5	94.4	95.3
		Deer	95.3	1.2	94.9	94.6
		Bird	95.4	5.0	94.6	97.3
		Horse	95.0	16.6	94.9	90.8
		Cat	95.2	12.5	94.3	87.8
		Dog	95.0	9.6	94.5	96.1

sacrificing test accuracy to learn more robust features after the new training samples are perturbed against the gradient of the loss function, a phenomenon also observed in adversarially trained classifiers [30].

Experiments on 5% poison ratio (Appendix Table 16 & 17) and on VGG19 (Appendix Table 18 & 19) similarly display the effectiveness of our defense.

8.3. Comparison with Baseline Defences

8.3.1 Detection of Poisoned Samples

When compared with another poison detection baseline called Activation Clustering (AC) [6] and we observe that our method is more robust in the detection of poisoned samples (Table 3 and 4). For full-sized overlay poison attacks, ACs sensitivity (accuracy of detecting poisoned samples) is $< 50\%$ for 4 out of the 9 CIFAR10 poison pairs in our experiments while our proposed detection method shows high sensitivity ($> 85\%$) consistently (Table 3). For the 9 small-

sized dot poison attacks, there are 3 pairs where AC detects poisoned samples with accuracy $< 60\%$ (sensitivity) while our proposed method shows comparatively high sensitivity ($> 80\%$) for all the poison pairs (Table 4). Since images from different CIFAR-10 classes (like cats and dogs) may look semantically more similar to one another than those from datasets evaluated in [6] like MNIST and LISA, we speculate that the activations of poisoned samples closely resemble those of clean samples despite being originally from different class labels. As a result, it is challenging to separate them with AC which relies on differences between activations of poisoned and clean target class samples. In contrast, our proposed method detects poisoned samples through their input gradients similarity with the extracted poison signal. This decouples the inter-class activation similarity problem from the detection of poisoned samples, thus explaining the more robust performance of our method.

Table 2. Accuracy on full test set and poisoned base class test images, before and after neutralization (Neu.) for dot poison.





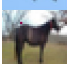




Sample	Target	Acc Before Neu. (%)		Acc After Neu. (%)	
		All	Poisoned	All	Poisoned
	Dog	95.4	0.5	94.9	87.5
	Frog	95.4	0.4	95.0	95.9
	Cat	95.3	0.4	95.2	86.0
	Bird	95.2	1.0	95.0	96.3
	Deer	95.3	0.5	95.1	96.4
	Bird	95.3	2.0	95.3	96.4
	Horse	95.3	1.0	94.6	81.4
	Cat	95.1	1.4	95.0	90.6
	Dog	95.4	3.0	95.2	98.2

Table 3. Full overlay poison detection (Specificity/Sensitivity) comparison with Activation Clustering (AC) [6] defense. Specificity is the accuracy of clean sample classification while sensitivity is the accuracy of poisoned sample classification.

Poison Pair #	1	2	3	4	5	6	7	8	9
Ours (%)	99.4 / 94.6	99.6 / 96.0	99.2 / 95.6	99.7 / 89.8	97.5 / 87.4	99.5 / 95.4	98.9 / 95.8	99.7 / 89.2	99.6 / 93.6
AC (%)	70.7 / 46.6	73.4 / 96.2	99.8 / 93.4	50.6 / 13.0	72.4 / 70.8	68.4 / 79.8	59.2 / 6.4	50.0 / 45.2	99.8 / 94.2

Table 4. Dot-sized poison detection (Specificity/Sensitivity) comparison with Activation Clustering (AC) defense.

Poison Pair #	1	2	3	4	5	6	7	8	9
Ours (%)	99.6 / 92.8	99.5 / 88.6	99.7 / 99.0	96.8 / 84.4	99.9 / 99	99.7 / 100	99.1 / 95.8	99.3 / 94	99.52 / 99.8
AC (%)	71.7 / 80.0	65.3 / 92.0	99.4 / 97.4	53.4 / 25.4	85.8 / 92.4	59.7 / 44.6	72.3 / 97.2	64.9 / 59.0	99.7 / 91.0

8.3.2 Final Neutralization

Other backdoor defense approaches such as [29, 16, 32] assume either prior knowledge about the attack’s target class and poison ratio or the availability of a verified clean dataset which makes it different from the more challenging threat model considered in this paper. Nonetheless, on experiments with the same poison parameters, our method is competitive (Table 5), compared to the defense in [29].

Table 5. Post-defense poison success rate (lower is better) comparison of full neutralization pipeline with spectral signature (SS) filtering [29] for 10% dot poison ratio.

Poison Pair #	1	2	3	4	5	6	7	8	9
Ours (%)	6.0	0	3.7	0.4	0.4	0.1	6.1	5.4	0
SS (%)	7.2	0.1	0.1	1.1	1.7	0.4	0.7	6.7	0

9. Conclusions

In this paper, we propose a comprehensive defense to counter backdoor attacks on neural networks. We show how

poison signals can be extracted from input gradients of poisoned training samples. With the insights that the principal components of input gradients from poisoned and clean samples form distinct clusters, we propose a method to detect the presence of backdoor poisoning, along with the corresponding poison target and base class. We then use the extracted poison signals to filter poisoned from clean samples in the target class. Finally, we retrain the model on an augmented dataset, which dissociates the poison signals from the target class, and show that it can effectively neutralize the backdoor for both large- and small-sized poisons in the CIFAR10 dataset without prior assumption on the poison classes and size. Comparison with baselines demonstrates both our approach’s superior poison detection and its competitiveness with existing methods even under a more challenging threat model. Our method consists of several key modules, each of which can potentially be a building block of more effective defenses in the future.

References

- [1] Yossi Adi, Carsten Baum, Moustapha Cisse, Benny Pinkas, and Joseph Keshet. Turning your weakness into a strength: Watermarking deep neural networks by backdooring. In *27th {USENIX} Security Symposium ({USENIX} Security 18)*, pages 1615–1631, 2018.
- [2] Anish Athalye, Nicholas Carlini, and David Wagner. Obfuscated gradients give a false sense of security: Circumventing defenses to adversarial examples. *arXiv preprint arXiv:1802.00420*, 2018.
- [3] Anish Athalye, Logan Engstrom, Andrew Ilyas, and Kevin Kwok. Synthesizing robust adversarial examples. *arXiv preprint arXiv:1707.07397*, 2017.
- [4] Battista Biggio, Blaine Nelson, and Pavel Laskov. Poisoning attacks against support vector machines. *arXiv preprint arXiv:1206.6389*, 2012.
- [5] Nicholas Carlini, Pratyush Mishra, Tavish Vaidya, Yuankai Zhang, Micah Sherr, Clay Shields, David Wagner, and Wenchao Zhou. Hidden voice commands. In *25th {USENIX} Security Symposium ({USENIX} Security 16)*, pages 513–530, 2016.
- [6] Bryant Chen, Wilka Carvalho, Nathalie Baracaldo, Heiko Ludwig, Benjamin Edwards, Taesung Lee, Ian Molloy, and Biplav Srivastava. Detecting backdoor attacks on deep neural networks by activation clustering. *arXiv preprint arXiv:1811.03728*, 2018.
- [7] Xinyun Chen, Chang Liu, Bo Li, Kimberly Lu, and Dawn Song. Targeted backdoor attacks on deep learning systems using data poisoning. *arXiv preprint arXiv:1712.05526*, 2017.
- [8] Kevin Eykholt, Ivan Evtimov, Earlene Fernandes, Bo Li, Amir Rahmati, Chaowei Xiao, Atul Prakash, Tadayoshi Kohno, and Dawn Song. Robust physical-world attacks on deep learning models. *arXiv preprint arXiv:1707.08945*, 2017.
- [9] Ian J Goodfellow, Jonathon Shlens, and Christian Szegedy. Explaining and harnessing adversarial examples. *arXiv preprint arXiv:1412.6572*, 2014.
- [10] Tianyu Gu, Brendan Dolan-Gavitt, and Siddharth Garg. Badnets: Identifying vulnerabilities in the machine learning model supply chain. *arXiv preprint arXiv:1708.06733*, 2017.
- [11] Kaiming He, Xiangyu Zhang, Shaoqing Ren, and Jian Sun. Deep residual learning for image recognition. In *Proceedings of the IEEE conference on computer vision and pattern recognition*, pages 770–778, 2016.
- [12] Pang Wei Koh and Percy Liang. Understanding black-box predictions via influence functions. In *Proceedings of the 34th International Conference on Machine Learning-Volume 70*, pages 1885–1894. JMLR. org, 2017.
- [13] Alex Krizhevsky and Geoffrey Hinton. Learning multiple layers of features from tiny images. Technical report, Cite-seer, 2009.
- [14] Alexey Kurakin, Ian Goodfellow, and Samy Bengio. Adversarial machine learning at scale. *arXiv preprint arXiv:1611.01236*, 2016.
- [15] Yann LeCun, Yoshua Bengio, and Geoffrey Hinton. Deep learning. *nature*, 521(7553):436, 2015.
- [16] Kang Liu, Brendan Dolan-Gavitt, and Siddharth Garg. Fine-pruning: Defending against backdooring attacks on deep neural networks. In *International Symposium on Research in Attacks, Intrusions, and Defenses*, pages 273–294. Springer, 2018.
- [17] Yingqi Liu, Shiqing Ma, Yousra Aafer, Wen-Chuan Lee, Juan Zhai, Weihang Wang, and Xiangyu Zhang. Trojaning attack on neural networks. In *25th Annual Network and Distributed System Security Symposium, NDSS 2018, San Diego, California, USA, February 18-22, 2018*. The Internet Society, 2018.
- [18] Aleksander Madry, Aleksandar Makelov, Ludwig Schmidt, Dimitris Tsipras, and Adrian Vladu. Towards deep learning models resistant to adversarial attacks. *arXiv preprint arXiv:1706.06083*, 2017.
- [19] Shike Mei and Xiaojin Zhu. The security of latent dirichlet allocation. In *Artificial Intelligence and Statistics*, pages 681–689, 2015.
- [20] Blaine Nelson, Marco Barreno, Fuching Jack Chi, Anthony D Joseph, Benjamin IP Rubinstein, Udam Saini, Charles A Sutton, J Doug Tygar, and Kai Xia. Exploiting machine learning to subvert your spam filter. *LEET*, 8:1–9, 2008.
- [21] Nicolas Papernot, Ian Goodfellow, Ryan Sheatsley, Reuben Feinman, and Patrick McDaniel. cleverhans v1. 0.0: an adversarial machine learning library. *arXiv preprint arXiv:1610.00768*, 10, 2016.
- [22] Mark Rudelson. Random vectors in the isotropic position. *Journal of Functional Analysis*, 164(1):60–72, 1999.
- [23] Jürgen Schmidhuber. Deep learning in neural networks: An overview. *Neural networks*, 61:85–117, 2015.
- [24] Ali Shafahi, W Ronny Huang, Mahyar Najibi, Octavian Suciu, Christoph Studer, Tudor Dumitras, and Tom Goldstein. Poison frogs! targeted clean-label poisoning attacks on neural networks. In *Advances in Neural Information Processing Systems*, pages 6103–6113, 2018.
- [25] Mahmood Sharif, Sruti Bhagavatula, Lujo Bauer, and Michael K Reiter. Accessorize to a crime: Real and stealthy attacks on state-of-the-art face recognition. In *Proceedings of the 2016 ACM SIGSAC Conference on Computer and Communications Security*, pages 1528–1540. ACM, 2016.
- [26] Karen Simonyan and Andrew Zisserman. Very deep convolutional networks for large-scale image recognition. *arXiv preprint arXiv:1409.1556*, 2014.
- [27] Jacob Steinhardt, Pang Wei W Koh, and Percy S Liang. Certified defenses for data poisoning attacks. In *Advances in neural information processing systems*, pages 3517–3529, 2017.
- [28] Florian Tramèr, Alexey Kurakin, Nicolas Papernot, Ian Goodfellow, Dan Boneh, and Patrick McDaniel. Ensemble adversarial training: Attacks and defenses. *arXiv preprint arXiv:1705.07204*, 2017.
- [29] Brandon Tran, Jerry Li, and Aleksander Madry. Spectral signatures in backdoor attacks. In *Advances in Neural Information Processing Systems*, pages 8011–8021, 2018.
- [30] Dimitris Tsipras, Shibani Santurkar, Logan Engstrom, Alexander Turner, and Aleksander Madry. Robustness may be at odds with accuracy. *stat*, 1050:11, 2018.

- [31] Roman Vershynin. *High-dimensional probability: An introduction with applications in data science*, volume 47. Cambridge University Press, 2018.
- [32] Bolun Wang, Yuanshun Yao, Shawn Shan, Huiying Li, Bimal Viswanath, Haitao Zheng, and Ben Y Zhao. Neural cleanse: Identifying and mitigating backdoor attacks in neural networks. In *Neural Cleanse: Identifying and Mitigating Backdoor Attacks in Neural Networks*, page 0. IEEE, 2019.
- [33] Eric Wong, Frank R Schmidt, and J Zico Kolter. Wasserstein adversarial examples via projected sinkhorn iterations. *arXiv preprint arXiv:1902.07906*, 2019.
- [34] Huang Xiao, Battista Biggio, Blaine Nelson, Han Xiao, Claudia Eckert, and Fabio Roli. Support vector machines under adversarial label contamination. *Neurocomputing*, 160:53–62, 2015.

A. Poison Signals in Input Gradients

A.1. Constructing a Backdoor

A.1.1 A Binary Classification Example

Our example considers clean data samples (\mathbf{x}, y) from a distribution D_c such that:

$$y \in \{-1, +1\}, \quad x_1 \sim \mathcal{N}(0, 1), \quad x_2, \dots, x_{d+1} \sim \mathcal{N}(\eta y, 1)$$

where x_i are independent and $\mathcal{N}(\mu, \sigma^2)$ is gaussian distribution with mean μ and variance σ^2 . In this dataset, the features x_2, \dots, x_{d+1} are correlated with the label y whereas x_1 is uncorrelated at all. We denote $(\mathbf{x}_-, -1)$ for samples with label -1 and $(\mathbf{x}_+, -1)$ for sample with label $+1$.

We can consider a simple neural network classifier f_c with a hidden layer made up of two neurons and RELU activation function g which is able to achieve high accuracy for D_c :

$$a_1^1 = \mathbf{w}_1^1 \top \mathbf{x} + b_1^1, \quad a_2^1 = \mathbf{w}_2^1 \top \mathbf{x} + b_2^1, \\ f_c(\mathbf{x}) := \text{sign}(w_1^2 g(a_1^1) + w_2^2 g(a_2^1))$$

where $\mathbf{w}_1^1 = [0, -\frac{1}{d}, \dots, -\frac{1}{d}]$, $b_1^1 = 0$, $\mathbf{w}_2^1 = [0, \frac{1}{d}, \dots, \frac{1}{d}]$, $b_2^1 = 0$, $w_1^2 = -1$, $w_2^2 = 1$. Considering the accuracy of f_c on D_c ,

$$\begin{aligned} \Pr\{f_c(\mathbf{x}) = y\} &= \Pr\{\text{sign}(w_1^2 g(\mathbf{w}_1^1 \top \mathbf{x}) + w_2^2 g(\mathbf{w}_2^1 \top \mathbf{x})) = y\} \\ &= \Pr\left\{\frac{y}{d} \sum_{i=1}^d \mathcal{N}_i(\eta y, 1) > 0\right\} \end{aligned} \quad (3)$$

where \mathcal{N}_i are independent gaussian distributions. Further simplifying it, we get

$$\begin{aligned} \Pr\{f_c(x) = y\} &= \Pr\left\{\mathcal{N}(\eta, \frac{1}{d}) > 0\right\} \\ &= \Pr\left\{\mathcal{N}(0, 1) > -\eta\sqrt{d}\right\} \end{aligned} \quad (4)$$

From this, we can observe that the accuracy of f_c is $>99.8\%$ on D_c when $\eta \geq \frac{3}{\sqrt{d}}$. f_c can have m times more similar neurons in the hidden layer and get similarly high training accuracy for D_c .

A.1.2 Effect of Poisoned Data on Learned Weights

We now consider a distribution of poisoned data $D = D_c \cup D_p$ which forms in a victim classifier f_p a backdoor after training. We study the case where an adversary forms a backdoor that causes f_p to misclassify \mathbf{x}_- samples as $+1$ when the poison signal is present. We denote the input-label pairs from D_p as (\mathbf{x}_p, y_p) :

$$y_p = +1, \quad x_1 = \psi, \quad x_2, \dots, x_{d+1} \sim \mathcal{N}(-\eta, 1) \quad (5)$$

where the poison signal is planted in x_1 with value $\psi > 0$ and y_p is mislabeled as the target label $+1$. Note that \mathbf{x}_p and \mathbf{x}_- are similar in their distribution except for their x_1 values which contains the poison signal for \mathbf{x}_p . If we use the same classifier f_c from § A.1.1, $f_c(\mathbf{x}_p) = -1 \neq y_p$, resulting in classification ‘error’ for most \mathbf{x}_p . With ε being the ratio of D_p samples in D , f_c would have ‘error’ rate of $\approx \varepsilon$ for D .

For high training accuracy on D , we study another neural network classifier f_p with a hidden layer made up of three different neurons and RELU activation function g :

$$a_1^1 = \mathbf{w}_1^1 \top \mathbf{x} + b_1^1, \quad a_2^1 = \mathbf{w}_2^1 \top \mathbf{x} + b_2^1, \quad a_3^1 = \mathbf{w}_3^1 \top \mathbf{x} + b_3^1, \\ f_p(\mathbf{x}) := \text{sign}(w_1^2 g(a_1^1) + w_2^2 g(a_2^1) + w_3^2 g(a_3^1))$$

similar to f_c for the first two hidden neurons,

$$\mathbf{w}_1^1 = \left[0, -\frac{1}{d}, \dots, -\frac{1}{d}\right], \quad b_1^1 = 0,$$

$$\mathbf{w}_2^1 = \left[0, \frac{1}{d}, \dots, \frac{1}{d}\right], \quad b_2^1 = 0, w_1^2 = -1, \quad w_2^2 = 1,$$

For f_p ’s third hidden neuron,

$$\mathbf{w}_3^1 = \left[\frac{1}{d}, 0, \dots, 0\right], \quad b_3^1 = -c\frac{1}{d}, \quad w_3^2 > \frac{\eta d}{(\psi - c)}$$

where $c > 0$ and g is the RELU activation function. The negative sign of b_3^1 suppresses the activation of the third neuron (a_3^1) for clean \mathbf{x}_- samples. Without this, its noise value at x_1 could have cause a_3^1 to be positive and flip the sign of $f_p(\mathbf{x}_-)$ to positive.

We can express the training accuracy on \mathbf{x}_p as

$$\begin{aligned} \Pr\{f_c(\mathbf{x}_p) = +1\} &= \\ \Pr\{\text{sign}(w_1^2 g(a_1^1) + w_2^2 g(a_2^1) + w_3^2 g(a_3^1)) = +1\} \end{aligned} \quad (6)$$

Combining the definition of \mathbf{x}_p in (5) with observations in (3) and (4), we get

$$\begin{aligned} \Pr\{f_c(\mathbf{x}_p) = +1\} &= \Pr\left\{\mathcal{N}\left(-\eta, \frac{1}{d}\right) + w_3^2(\psi - c)\frac{1}{d} > 0\right\} \\ &= \Pr\left\{\mathcal{N}(0, 1) > \eta\sqrt{d} - (\psi - c)\frac{w_3^2}{\sqrt{d}}\right\} \end{aligned} \quad (7)$$

For the training accuracy of poisoned samples $\Pr\{f_c(\mathbf{x}_p) = +1\} > 0.5$, we need

$$\eta\sqrt{d} - (\psi - c)\frac{w_3^2}{\sqrt{d}} < 0$$

which is satisfied when

$$c_1 = (\psi - c) > 0 \text{ and } (\psi - c)\frac{w_3^2}{\sqrt{d}} > \eta\sqrt{d}$$

From here, we can deduce that for high training accuracy of poisoned samples, we need

$$c_1 \frac{w_3^2}{\sqrt{d}} \gg \eta \sqrt{d} \text{ which implies } w_3^2 \gg \frac{1}{c_1} \eta d$$

Combining with the result from (4) that $\eta \geq \frac{C}{\sqrt{d}}$ is needed for high training accuracy of \mathbf{x}_- and \mathbf{x}_+ , we get $w_3^2 \gg c_2 \sqrt{d}$. When d is large for high dimensional inputs,

$$w_3^2 \gg c_2 \sqrt{d} > 1 = |w_1^2|, |w_2^2| \quad (8)$$

This means that the weight of third neuron representing poisoned input feature would be much larger than that of the first and second neurons representing normal input features. In practice, poison feature neurons having larger weight values than clean feature neurons of deep neural networks is observed empirically in other data poisoning studies (cite papers).

During inference, most $\mathbf{x}_p \in D$ would result in positive a_1^1 and a_3^1 while a_2^1 would be negative. The corresponding activation values for \mathbf{x}_- and \mathbf{x}_+ in f_p are summarized in Table 6.

Table 6. Signs of f_p activations and the corresponding partial derivative (g') of RELU function.

	a_1^1	a_2^1	a_3^1	$g(a_1^1)$	$g(a_2^1)$	$g(a_3^1)$	$g'(a_1^1)$	$g'(a_2^1)$	$g'(a_3^1)$
\mathbf{x}_-	+	-	-	+	0	0	1	0	0
\mathbf{x}_+	-	+	-	0	+	0	0	1	0
\mathbf{x}_p	+	-	+	+	0	+	1	0	1

Since the RELU activation function is $g(x) = \begin{cases} x, & x > 0 \\ 0, & x < 0 \end{cases}$ and its derivative is $g'(x) = \begin{cases} 1, & x > 0 \\ 0, & x < 0 \end{cases}$, we can calculate the post-RELU activation values and their derivative, also summarized in Table 6. The poisoned inputs \mathbf{x}_p have different profile of neuron activation from the clean inputs \mathbf{x}_- and \mathbf{x}_+ . More specifically, f_p 's third neuron is only activated by inputs with poison signal $x_1 = \psi$, like \mathbf{x}_p . Combining these insights about a poisoned classifier model's 'poison' neuron weights and activations with § A.2, we propose a method to recover poison signals in the input layer, detect poison target class and, subsequently, poisoned images.

A.2. Poison Signal in Input Gradients

Proposition A.1. *The gradient of loss function E with respect to the input x_i is linearly dependent on activated neurons' weights such that*

$$\frac{\partial E}{\partial x_i} = \sum_{j=1}^{r_1} \left[w_{ij}^1 g'(a_j^1) \sum_{l=1}^{r_2} \delta_l^2 w_{jl}^2 \right] \quad (9)$$

where $\delta_j^k \equiv \frac{\partial E}{\partial a_j^k}$ usually called the error, is the derivative of E with respect to activation a_j^k for neuron node i in layer

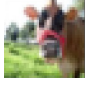
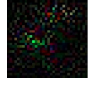
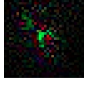
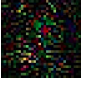
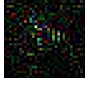
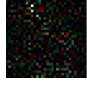
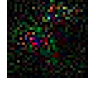
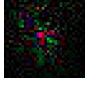
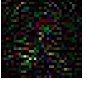
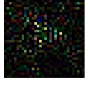

k . w_{ij}^k is the weight for node j in layer k for incoming node i , r_k is the number of nodes in layer k , g is the activation function for the hidden layer nodes and g' is its derivative.

The detailed proof of this proposition is in Appendix B. The gradient with respect to the input x_i is linearly dependent on the w_{ij}^1 , $g'(a_j^1)$ and w_{jl}^2 terms. The value of δ_l^2 is dependent on the loss function of the classifier model and the activations of the neural networks in deeper layers. In f_p , δ_l^2 is simply ± 1 meaning that $|\delta_l^2| = 1$, we can get

$$\left| \frac{\partial E}{\partial x_i} \right| = \sum_{j=1}^3 [w_{ij}^1 g'(a_j^1) w_j^2] \quad (10)$$

We know the values of $g'(a_j^1)$ from Table 6. Since $g'(a_3^1) = 0$ for most \mathbf{x}_- and \mathbf{x}_+ , $\left| \frac{\partial E}{\partial x_1} \right|$ will be much larger for poisoned samples \mathbf{x}_p than for clean samples, \mathbf{x}_- and \mathbf{x}_+ . Moreover, from (8) we know that the weight of 'poison' neurons (w_3^2) are much larger than weight of 'clean' neurons (w_1^2 and w_2^2) when d is large, resulting in $\left| \frac{\partial E}{\partial x_1} \right| \gg \left| \frac{\partial E}{\partial x_i} \right|, \forall i \neq 1$. Informally, this means that there will be a relatively large absolute gradient value at the poison signal's input positions (x_1) of poisoned inputs (\mathbf{x}_p) compared to other input positions. In practice, when we directly compare the gradients of poisoned samples with those of clean samples, shown in Table 7, the gradients are too noisy to discern poison signals. In § 4.2, we show how we filter these input poison signals and use them to separate poisoned from clean samples with guarantees in § 5.

Table 7. Gradients of randomly drawn poisoned and clean inputs with respect to the loss function. The poisoned target and base class are ‘Dog’ and ‘Cat’ respectively from the CIFAR10 dataset. Poisoned samples are overlaid with 20% of the poison image. The positive and negative components of the input gradients and illustrated separately and normalized by the maximum value of the gradient at each pixel position.

Poison	Gradient of Poisoned Inputs			Gradient of Clean Inputs		
	+					
	-					

B. Proof of Proposition 4.1

Proposition B.1. *The gradient of loss function E with respect to the input x_i is linearly dependent on activated neurons’ weights such that*

$$\frac{\partial E}{\partial x_i} = \sum_{j=1}^{r_1} \left[w_{ij}^1 g'(a_j^1) \sum_{l=1}^{r_2} \delta_l^2 w_{jl}^2 \right] \quad (11)$$

where $\delta_j^k \equiv \frac{\partial E}{\partial a_j^k}$ usually called the error, is the derivative of loss function E with respect to activation a_j^k for neuron node j in layer k . w_{ij}^k is the weight for node j in layer k for incoming node i , r_k is the number of nodes in layer k , g is the activation function for the hidden layer nodes and g' is its derivative.

Proof. We denote o_i^k as the output for node i in layer k . For simplicity, the bias for node i in layer k is denoted as a weight w_{0j}^k with fixed output $o_i^{k-1} = 1$ for node 0 in layer $k-1$.

For $k = m$ where m is the final layer,

$$\frac{\partial E}{\partial o_i^{k-1}} = \frac{\partial E}{\partial a_j^k} \frac{\partial a_j^k}{\partial o_i^{k-1}}$$

$$a_j^k = \sum_{l=0}^{r_{k-1}} w_{ij}^k o_l^{k-1}$$

$$\frac{\partial a_j^k}{\partial o_i^{k-1}} = w_{ij}^k$$

$$\frac{\partial E}{\partial o_i^{k-1}} = \delta_j^k w_{ij}^k$$

where

$$\delta_j^k \equiv \frac{\partial E}{\partial a_j^k}$$

For $1 \leq k < m$,

$$\frac{\partial E}{\partial o_i^{k-1}} = \sum_{j=1}^{r_k} \frac{\partial E}{\partial a_j^k} \frac{\partial a_j^k}{\partial o_i^{k-1}} = \sum_{j=1}^{r_k} \delta_j^k w_{ij}^k \quad (12)$$

With chain rule for multivariate functions,

$$\begin{aligned} \delta_j^k &\equiv \frac{\partial E}{\partial a_j^k} = \sum_{l=1}^{r_{k+1}} \frac{\partial E}{\partial a_l^{k+1}} \frac{\partial a_l^{k+1}}{\partial a_j^k} \\ &= \sum_{l=1}^{r_{k+1}} \delta_l^{k+1} \frac{\partial a_l^{k+1}}{\partial a_j^k} \end{aligned} \quad (13)$$

With definition of a_l^{k+1} ,

$$a_l^{k+1} = \sum_{i=0}^{r_k} w_{il}^{k+1} g(a_j^k)$$

where $g(x)$ is the activation function.

Taking partial derivative with respect to a_j^k , we get

$$\frac{\partial a_l^{k+1}}{\partial a_j^k} = w_{jl}^{k+1} g'(a_j^k) \quad (14)$$

Substituting (14) into (13), we get

$$\begin{aligned} \delta_j^k &= \sum_{l=1}^{r_{k+1}} \delta_l^{k+1} w_{jl}^{k+1} g'(a_j^k) \\ &= g'(a_j^k) \sum_{l=1}^{r_{k+1}} \delta_l^{k+1} w_{jl}^{k+1} \end{aligned} \quad (15)$$

Finally, substituting (15) into (12), we get

$$\frac{\partial E}{\partial o_i^{k-1}} = \sum_{j=1}^{r_k} \left[w_{ij}^k g'(a_j^k) \sum_{l=1}^{r_{k+1}} \delta_l^{k+1} w_{jl}^{k+1} \right] \quad (16)$$

□

C. Proof of Theorem 4.1 and 5.1

The second moment matrix of \mathbf{z} is denoted by

$$\Sigma = \mathbb{E} \mathbf{z} \mathbf{z}^\top$$

By further expanding this, we get,

$$\Sigma = \mathbb{E} \left(\frac{1}{N} \begin{bmatrix} g_{11} & \cdots & g_{N1} + \mu_1 \\ \vdots & \ddots & \vdots \\ g_{1n} & \cdots & g_{Nn} + \mu_n \end{bmatrix} \begin{bmatrix} g_{11} & \cdots & g_{1n} \\ \vdots & \ddots & \vdots \\ g_{N1} + \mu_1 & \cdots & g_{nn} + \mu_n \end{bmatrix} \right) \quad (17)$$

Since $\mathbb{E}(\mathbf{Z}_{ij}) = (\mathbb{E} \mathbf{Z})_{ij}$, $\mathbb{E} g_i g_j = \begin{cases} \eta, & i = j \\ 0, & i \neq j \end{cases}$ and $\mathbb{E} g = 0$, we get

$$\begin{aligned} \Sigma &= \frac{1}{N} \left(\begin{bmatrix} 0 & \cdots & \mu_1 \\ \vdots & \ddots & \vdots \\ 0 & \cdots & \mu_n \end{bmatrix} \begin{bmatrix} 0 & \cdots & 0 \\ \vdots & \ddots & \vdots \\ \mu_1 & \cdots & \mu_n \end{bmatrix} \right) + \eta \mathbf{I}_n \\ &= \varepsilon \begin{bmatrix} \mu_1^2 & \cdots & \mu_1 \mu_n \\ \vdots & \ddots & \vdots \\ \mu_1 \mu_n & \cdots & \mu_n^2 \end{bmatrix} + \eta \mathbf{I}_n \end{aligned} \quad (18)$$

Theorem C.1. μ is the eigenvector of Σ and corresponds to the largest eigenvalue if ε and $\|\mu\|_2$ are both > 0 .

Proof. Taking the matrix multiplication of Σ and μ , we get

$$\begin{aligned} \Sigma \mu &= \varepsilon \begin{bmatrix} \mu_1^2 & \cdots & \mu_1 \mu_n \\ \vdots & \ddots & \vdots \\ \mu_1 \mu_n & \cdots & \mu_n^2 \end{bmatrix} \begin{bmatrix} \mu_1 \\ \vdots \\ \mu_n \end{bmatrix} + \eta \mathbf{I}_n \begin{bmatrix} \mu_1 \\ \vdots \\ \mu_n \end{bmatrix} \\ &= \varepsilon \begin{bmatrix} \mu_1^3 + \mu_1 \mu_2^2 + \cdots + \mu_1 \mu_n^2 \\ \vdots \\ \mu_1^2 \mu_n + \mu_2^2 \mu_n + \cdots + \mu_n^3 \end{bmatrix} + \eta \begin{bmatrix} \mu_1 \\ \vdots \\ \mu_n \end{bmatrix} \\ &= \varepsilon (\mu_1^2 + \cdots + \mu_n^2) \begin{bmatrix} \mu_1 \\ \vdots \\ \mu_n \end{bmatrix} + \eta \begin{bmatrix} \mu_1 \\ \vdots \\ \mu_n \end{bmatrix} \\ &= (\varepsilon \|\mu\|_2^2 + \eta) \begin{bmatrix} \mu_1 \\ \vdots \\ \mu_n \end{bmatrix} \\ &= (\varepsilon \|\mu\|_2^2 + \eta) \mu \end{aligned} \quad (19)$$

Thus, μ is an eigenvector of Σ with eigenvalue $\lambda_1(\Sigma) = \varepsilon \|\mu\|_2^2 + \eta$. Next, we proceed to prove that $\lambda_1(\Sigma)$ is the largest eigenvalue.

$$\text{Let } \mathbf{D} = \varepsilon \begin{bmatrix} \mu_1^2 & \cdots & \mu_1 \mu_n \\ \vdots & \ddots & \vdots \\ \mu_1 \mu_n & \cdots & \mu_n^2 \end{bmatrix},$$

then we can express Σ as

$$\Sigma = \mathbf{D} + \eta \mathbf{I}_n \quad (20)$$

Similar to (19), we can get

$$\begin{aligned} \mathbf{D} \mu &= \varepsilon \begin{bmatrix} \mu_1^2 & \cdots & \mu_1 \mu_n \\ \vdots & \ddots & \vdots \\ \mu_1 \mu_n & \cdots & \mu_n^2 \end{bmatrix} \begin{bmatrix} \mu_1 \\ \vdots \\ \mu_n \end{bmatrix} \\ &= \varepsilon \begin{bmatrix} \mu_1^3 + \mu_1 \mu_2^2 + \cdots + \mu_1 \mu_n^2 \\ \vdots \\ \mu_1^2 \mu_n + \mu_2^2 \mu_n + \cdots + \mu_n^3 \end{bmatrix} \\ &= \varepsilon (\mu_1^2 + \cdots + \mu_n^2) \begin{bmatrix} \mu_1 \\ \vdots \\ \mu_n \end{bmatrix} \\ &= (\varepsilon \|\mu\|_2^2) \mu \end{aligned} \quad (21)$$

This shows that μ is also an eigenvector of \mathbf{D} with eigenvalue $\lambda_1(\mathbf{D}) = \varepsilon \|\mu\|_2^2$.

From (18), we observe that \mathbf{D} is a product of a matrix by its own transpose. This implies that \mathbf{D} is positive semi-definite and all its eigenvalues are non-negative. Furthermore, the sum of all these eigenvalues is

$$\begin{aligned} \sum_{i=1}^n \lambda_i(\mathbf{D}) &= \text{tr}(\mathbf{D}) \\ &= \varepsilon \|\mu\|_2^2 \\ &= \lambda_1(\mathbf{D}) \end{aligned} \quad (22)$$

This implies that the other eigenvalues $\lambda_2(\mathbf{D}) = \cdots = \lambda_n(\mathbf{D}) = 0$. From this, we know that all vectors \mathbf{v} which are orthogonal to μ ,

$$\forall \mathbf{v} \in \mathbb{R}^n : \langle \mathbf{v}, \mu \rangle = 0$$

$$\mathbf{D} \mathbf{v} = \mathbf{0}$$

Combining with (20), we get

$$\begin{aligned} \Sigma \mathbf{v} &= \mathbf{D} \mathbf{v} + \eta \mathbf{I}_n \mathbf{v} \\ &= \eta \mathbf{v} \end{aligned} \quad (23)$$

With this, we can deduce that Σ 's other eigenvalues $\lambda_2(\Sigma) = \cdots = \lambda_n(\Sigma) = \eta$.

For $\lambda_1(\Sigma)$ to be the largest eigenvalue, this statement has to be true:

$$\lambda_1(\Sigma) > \max_{i \neq 1} \lambda_i(\Sigma)$$

With our previous calculations of $\lambda_i(\Sigma)$ in (19) and (23), we get

$$\begin{aligned}\varepsilon \|\mu\|_2^2 + \eta &> \eta \\ \varepsilon \|\mu\|_2 &> 0\end{aligned}\quad (24)$$

This statement is true if $\varepsilon > 0$ and $\|\mu\|_2 > 0$ which completes the proof. \square

Remark C.1.1. The operator or spectral norm of Σ , $\|\Sigma\|$, equals to the absolute value of its largest singular value. Since Σ is a positive semi-definite matrix, its largest singular value is the same as its largest eigenvalue. This implies that

$$\|\Sigma\| = \varepsilon \|\mu\|_2^2 + \eta \quad (25)$$

Theorem C.2 (Matrix Bernstein [31]). Let $\mathbf{Z}_1, \dots, \mathbf{Z}_N$ be symmetric $n \times n$ random matrices. Assume that $\|\mathbf{Z}_i\| \leq K$ almost surely and let $\|\sum_i \mathbf{Z}_i^2\| \leq \sigma^2$. Then,

$$Pr\left\{\left\|\sum_i \mathbf{Z}_i\right\| > t\right\} \leq 2n \exp\left(-c \min\left\{\frac{t^2}{\sigma^2}, \frac{t}{K}\right\}\right)$$

where $c > 0$ is an absolute constant.

Theorem C.3 (Covariance Estimation [22]). Let $\Sigma = \mathbb{E} \mathbf{z} \mathbf{z}^\top$ be the second moment matrix of \mathbb{R}^n random vector \mathbf{z} . With independent samples $\mathbf{z}_1, \dots, \mathbf{z}_N$, $\Sigma_N = \frac{1}{N} \sum_i \mathbf{z}_i \mathbf{z}_i^\top$ is the unbiased estimator of Σ . Assume that $\|\mathbf{z}_i\|_2^2 \leq M$. Then,

$$Pr\{\|\Sigma_N - \Sigma\| > \epsilon \|\Sigma\|\} \geq 1 - 2n \exp\left(-c_1 \frac{N \epsilon^2 \|\Sigma\|}{M + \|\Sigma\|}\right)$$

where $\epsilon \in (0, 1]$.

Proof. Let $\mathbf{Z}_i = \frac{1}{N} (\mathbf{z}_i \mathbf{z}_i^\top - \Sigma)$

Then,

$$\begin{aligned}\sum_{i=1}^N \mathbf{Z}_i &= \frac{1}{N} \sum_{i=1}^N \mathbf{z}_i \mathbf{z}_i^\top - \Sigma \\ &= \Sigma_N - \Sigma\end{aligned}\quad (26)$$

To apply Theorem C.3 to (26), we need to bound $\|\mathbf{Z}_i\|$ and $\|\sum_i \mathbf{Z}_i^2\|$.

To bound $\|\mathbf{Z}_i\|$,

$$\|\mathbf{Z}_i\| = \left\|\frac{1}{N} (\mathbf{z}_i \mathbf{z}_i^\top - \Sigma)\right\|$$

With triangle inequality, we get

$$\|\mathbf{Z}_i\| \leq \frac{1}{N} (\|\mathbf{z}_i \mathbf{z}_i^\top\| + \|\Sigma\|) \quad (27)$$

While considering the term $\|\mathbf{z}_i \mathbf{z}_i^\top\|$, we note that $\mathbf{z}_i \mathbf{z}_i^\top$ is a positive definite matrix. Then,

$$\begin{aligned}\|\mathbf{z} \mathbf{z}^\top\| &= \left\|\begin{bmatrix} z_1 \\ \vdots \\ z_n \end{bmatrix} \begin{bmatrix} z_1 & \cdots & z_n \end{bmatrix}\right\| \\ &= \left\|\begin{bmatrix} z_1^2 & \cdots & z_1 z_n \\ \vdots & \ddots & \vdots \\ z_1 z_n & \cdots & z_n^2 \end{bmatrix}\right\| \\ &= s_1(\mathbf{z} \mathbf{z}^\top) \\ &= \lambda_1(\mathbf{z} \mathbf{z}^\top) \\ &\leq \text{tr}(\mathbf{z} \mathbf{z}^\top) \\ &= z_1^2 + \cdots + z_n^2 \\ &= \|\mathbf{z}\|_2^2\end{aligned}\quad (28)$$

Substituting (28) into (27), we get

$$\|\mathbf{Z}_i\| \leq \frac{1}{N} (\|\mathbf{z}_i\|_2^2 + \|\Sigma\|)$$

Since $\|\mathbf{z}_i\|_2^2 \leq M$,

$$\|\mathbf{Z}_i\| \leq \frac{M + \|\Sigma\|}{N} = K \quad (29)$$

where K is the term from Theorem C.3.

To bound $\|\sum_i \mathbf{Z}_i^2\|$, we first expand \mathbf{Z}_i^2 .

$$\begin{aligned}\mathbf{Z}_i^2 &= \frac{1}{N^2} (\mathbf{z}_i \mathbf{z}_i^\top - \Sigma)^2 \\ &= \frac{1}{N^2} [(\mathbf{z}_i \mathbf{z}_i^\top)^2 - \Sigma(\mathbf{z}_i \mathbf{z}_i^\top) - (\mathbf{z}_i \mathbf{z}_i^\top) \Sigma + \Sigma^2]\end{aligned}\quad (30)$$

Taking expectation of both sides, we get

$$\begin{aligned}\mathbb{E} \mathbf{Z}_i^2 &= \frac{1}{N^2} [\mathbb{E}(\mathbf{z}_i \mathbf{z}_i^\top \mathbf{z}_i \mathbf{z}_i^\top) - \mathbb{E}[\Sigma(\mathbf{z}_i \mathbf{z}_i^\top)] - \mathbb{E}[(\mathbf{z}_i \mathbf{z}_i^\top) \Sigma] + \mathbb{E} \Sigma^2] \\ &= \frac{1}{N^2} [\mathbb{E}(\mathbf{z}_i \|\mathbf{z}_i\|_2^2 \mathbf{z}_i^\top) - \Sigma \mathbb{E}(\mathbf{z}_i \mathbf{z}_i^\top) - \mathbb{E}(\mathbf{z}_i \mathbf{z}_i^\top) \Sigma + \Sigma^2]\end{aligned}\quad (31)$$

Since $\|\mathbf{z}_i\|_2^2 \leq M$,

$$\mathbb{E} \mathbf{Z}_i^2 \preceq \frac{1}{N^2} [M \mathbb{E}(\mathbf{z}_i \mathbf{z}_i^\top) - \Sigma \mathbb{E}(\mathbf{z}_i \mathbf{z}_i^\top) - \mathbb{E}(\mathbf{z}_i \mathbf{z}_i^\top) \Sigma + \Sigma^2]$$

By definition, $\Sigma = \mathbb{E} \mathbf{z} \mathbf{z}^\top$

$$\begin{aligned}\mathbb{E} \mathbf{Z}_i^2 &\preceq \frac{1}{N^2} (M \Sigma - \Sigma \Sigma - \Sigma \Sigma + \Sigma^2) \\ &= \frac{1}{N^2} (M \Sigma - \Sigma^2)\end{aligned}\quad (32)$$

Thus,

$$\left\|\mathbb{E} \sum_{i=1}^N \mathbf{Z}_i^2\right\| = \left\|\frac{1}{N} (M \Sigma - \Sigma^2)\right\|$$

With triangle inequality, we get

$$\begin{aligned} \left\| \mathbb{E} \sum_{i=1}^N \mathbf{z}_i^2 \right\| &\leq \left\| \frac{M}{N} \boldsymbol{\Sigma} \right\| + \left\| \frac{1}{N} \boldsymbol{\Sigma}^2 \right\| \\ &= \frac{M \|\boldsymbol{\Sigma}\| + \|\boldsymbol{\Sigma}\|^2}{N} = \sigma^2 \end{aligned} \quad (33)$$

where σ^2 is the term from Theorem C.3.

Applying Theorem C.3 for $\sum_{i=1}^N \mathbf{z}_i$ with (29) and (33), and recalling from (26) where $\sum_{i=1}^N \mathbf{z}_i = \boldsymbol{\Sigma}_N - \boldsymbol{\Sigma}$, we get

$$\begin{aligned} &Pr\{\|\boldsymbol{\Sigma}_N - \boldsymbol{\Sigma}\| > \epsilon \|\boldsymbol{\Sigma}\|\} \\ &\leq 2n \exp \left(-c_1 \min \left\{ \frac{N\epsilon^2 \|\boldsymbol{\Sigma}\|^2}{M \|\boldsymbol{\Sigma}\| + \|\boldsymbol{\Sigma}\|^2}, \frac{N\epsilon \|\boldsymbol{\Sigma}\|}{M + \|\boldsymbol{\Sigma}\|} \right\} \right) \\ &= 2n \exp \left(-c_1 \min \left\{ \frac{N\epsilon^2 \|\boldsymbol{\Sigma}\|}{M + \|\boldsymbol{\Sigma}\|}, \frac{N\epsilon \|\boldsymbol{\Sigma}\|}{M + \|\boldsymbol{\Sigma}\|} \right\} \right) \end{aligned} \quad (34)$$

Assuming $\epsilon \in (0, 1]$,

$$Pr\{\|\boldsymbol{\Sigma}_N - \boldsymbol{\Sigma}\| > \epsilon \|\boldsymbol{\Sigma}\|\} \leq 2n \exp \left(-c_1 \frac{N\epsilon^2 \|\boldsymbol{\Sigma}\|}{M + \|\boldsymbol{\Sigma}\|} \right)$$

Thus,

$$Pr\{\|\boldsymbol{\Sigma}_N - \boldsymbol{\Sigma}\| \leq \epsilon \|\boldsymbol{\Sigma}\|\} \geq 1 - 2n \exp \left(-c_1 \frac{N\epsilon^2 \|\boldsymbol{\Sigma}\|}{M + \|\boldsymbol{\Sigma}\|} \right) \quad (35)$$

□

Theorem C.4 (Davis-Kahan Theorem). *Let \mathbf{S} and \mathbf{T} be symmetric matrices with same dimensions. Fix i and assume that the i th largest eigenvalue is well separated from the other eigenvalues:*

$$\min_{j:j \neq i} |\lambda_i(\mathbf{S}) - \lambda_j(\mathbf{S})| = \delta > 0$$

Then, the unit eigenvectors $\mathbf{v}_i(\mathbf{S})$ and $\mathbf{v}_i(\mathbf{T})$ are close to each other up to a sign.

$$\exists \theta \in \{-1, 1\} : \|\mathbf{v}_i(\mathbf{S}) - \theta \mathbf{v}_i(\mathbf{T})\|_2 \leq \frac{2^{\frac{2}{3}} \|\mathbf{S} - \mathbf{T}\|}{\delta}$$

Theorem C.5 (Guarantee of Poison Classification through Clustering). *Assume that all \mathbf{z}_i are normalized such that $\|\mathbf{z}_i\|_2 = 1$. Then the error probability of the poison clustering algorithm is given by*

$$\begin{aligned} &Pr \left\{ N_{error} \leq c_2 N \epsilon \left(\frac{1}{\|\mu\|_2} + \frac{\eta}{\epsilon \|\mu\|_2^3} \right) \right\} \geq \\ &1 - 2n \exp \left(-c_1 N \epsilon^2 \frac{(\epsilon \|\mu\|_2^2 + \eta)}{1 + \epsilon \|\mu\|_2^2 + \eta} \right) \end{aligned} \quad (36)$$

where N_{error} is the number of misclassified points and $\epsilon \in (0, 1]$.

Proof. To find the difference between unit eigenvectors $\mathbf{v}_1(\boldsymbol{\Sigma})$ and $\mathbf{v}_1(\boldsymbol{\Sigma}_N)$, we applying Theorem C.4 for $i = 1$, $\mathbf{S} = \boldsymbol{\Sigma}$, $\mathbf{T} = \boldsymbol{\Sigma}_N$,

$$\delta = \min_{j \neq 1} |\lambda_1(\boldsymbol{\Sigma}) - \lambda_j(\boldsymbol{\Sigma})|$$

With our previous calculations of $\lambda_i(\boldsymbol{\Sigma})$ in (19) and (23), we get

$$\begin{aligned} \delta &= \epsilon \|\mu\|_2^2 + \eta - \eta \\ &= \epsilon \|\mu\|_2^2 \end{aligned} \quad (37)$$

The conclusion of Theorem C.4 then becomes

$$\exists \theta \in \{-1, 1\} : \|\mathbf{v}_1(\boldsymbol{\Sigma}) - \theta \mathbf{v}_1(\boldsymbol{\Sigma}_N)\|_2 \leq \frac{2^{\frac{2}{3}}}{\epsilon \|\mu\|_2^2} \|\boldsymbol{\Sigma} - \boldsymbol{\Sigma}_N\|$$

Combining this with the Theorem C.3, we get

$$\begin{aligned} &Pr \left\{ \|\mathbf{v}_1(\boldsymbol{\Sigma}) - \theta \mathbf{v}_1(\boldsymbol{\Sigma}_N)\|_2 \leq \frac{2^{\frac{2}{3}}}{\epsilon \|\mu\|_2^2} \epsilon \|\boldsymbol{\Sigma}\| \right\} \geq \\ &1 - 2n \exp \left(-c_1 \frac{N\epsilon^2 \|\boldsymbol{\Sigma}\|}{M + \|\boldsymbol{\Sigma}\|} \right) \end{aligned} \quad (38)$$

We now have a probability bound of difference between $\mathbf{v}_1(\boldsymbol{\Sigma})$ and $\mathbf{v}_1(\boldsymbol{\Sigma}_N)$. To find the probability bound on the number of misclassified points, let us consider the case where \mathbf{z}_i is from a non-poisoned point.

If \mathbf{z}_i is from a poisoned point,

$$\begin{aligned} \mathbb{E} \langle \mu, \mathbf{z}_i \rangle &= \mathbb{E} \left([\mu_1 \ \cdots \ \mu_n] \begin{bmatrix} \mu_1 + g_1 \\ \vdots \\ \mu_n + g_n \end{bmatrix} \right) \\ &= \mathbb{E}(\mu_1^2 + g_1 \mu_1 + \cdots + \mu_n^2 + g_n \mu_n) \\ &= \mathbb{E}(\mu_1^2 + \cdots + \mu_n^2) + \mathbb{E}(g_1 \mu_1 + \cdots + g_n \mu_n) \\ &= \|\mu\|_2^2 \end{aligned} \quad (39)$$

Dividing by $\|\mu\|_2^2$ on both sides, we get

$$\mathbb{E} \left\langle \frac{\mu}{\|\mu\|_2}, \frac{\mathbf{z}_i}{\|\mu\|_2} \right\rangle = 1$$

From Theorem 4.1, since we know that μ is the first eigenvector of $\boldsymbol{\Sigma}$, $\frac{\mu}{\|\mu\|_2}$ is its first unit eigenvector $\mathbf{v}_1(\boldsymbol{\Sigma})$. Then,

$$\mathbb{E} \langle \mathbf{v}_1(\boldsymbol{\Sigma}), \frac{\mathbf{z}_i}{\|\mu\|_2} \rangle = 1 \quad (40)$$

If \mathbf{z}_i is from a non-poisoned point,

$$\begin{aligned}\mathbb{E}\langle \mathbf{v}_1(\mathbf{\Sigma}), \frac{\mathbf{z}_i}{\|\mu\|_2} \rangle &= \frac{1}{\|\mu\|_2^2} \mathbb{E} \left([\mu_1 \quad \cdots \quad \mu_n] \begin{bmatrix} g_1 \\ \vdots \\ g_n \end{bmatrix} \right) \\ &= \frac{1}{\|\mu\|_2^2} \mathbb{E}(g_1\mu_1 + \cdots + g_n\mu_n) \\ &= \frac{1}{\|\mu\|_2^2} \cdot 0 = 0\end{aligned}\tag{41}$$

Now, we consider the inner product of \mathbf{z}_i with the difference between $\mathbf{v}_1(\mathbf{\Sigma})$ and $\mathbf{v}_1(\mathbf{\Sigma}_N)$.

$$\mathbf{z}_i^\top \mathbf{v}_1(\mathbf{\Sigma}) - \theta \mathbf{z}_i^\top \mathbf{v}_1(\mathbf{\Sigma}_N) = \mathbf{z}_i^\top (\mathbf{v}_1(\mathbf{\Sigma}) - \theta \mathbf{v}_1(\mathbf{\Sigma}_N))$$

By Cauchy-Schwarz Inequality,

$$|\mathbf{z}_i^\top \mathbf{v}_1(\mathbf{\Sigma}) - \theta \mathbf{z}_i^\top \mathbf{v}_1(\mathbf{\Sigma}_N)| \leq \|\mathbf{z}_i\|_2 \cdot \|\mathbf{v}_1(\mathbf{\Sigma}) - \theta \mathbf{v}_1(\mathbf{\Sigma}_N)\|_2$$

By considering all the N samples of x_i ,

$$\sum_{i=1}^N |\mathbf{z}_i^\top \mathbf{v}_1(\mathbf{\Sigma}) - \theta \mathbf{z}_i^\top \mathbf{v}_1(\mathbf{\Sigma}_N)| \leq N \|\mathbf{z}_i\|_2 \cdot \|\mathbf{v}_1(\mathbf{\Sigma}) - \theta \mathbf{v}_1(\mathbf{\Sigma}_N)\|_2$$

Dividing by $\|\mu\|_2$ on both sides, we get

$$\begin{aligned}\sum_{i=1}^N \left| \frac{\mathbf{z}_i^\top}{\|\mu\|_2} \mathbf{v}_1(\mathbf{\Sigma}) - \theta \frac{\mathbf{z}_i^\top}{\|\mu\|_2} \mathbf{v}_1(\mathbf{\Sigma}_N) \right| &\leq \\ N \frac{\|\mathbf{z}_i\|_2}{\|\mu\|_2} \|\mathbf{v}_1(\mathbf{\Sigma}) - \theta \mathbf{v}_1(\mathbf{\Sigma}_N)\|_2\end{aligned}\tag{42}$$

$$\begin{aligned}\sum_{i=1}^N \left| \langle \mathbf{v}_1(\mathbf{\Sigma}), \frac{\mathbf{z}_i}{\|\mu\|_2} \rangle - \theta \langle \mathbf{v}_1(\mathbf{\Sigma}_N), \frac{\mathbf{z}_i}{\|\mu\|_2} \rangle \right| &\leq \\ N \frac{\|\mathbf{z}_i\|_2}{\|\mu\|_2} \|\mathbf{v}_1(\mathbf{\Sigma}) - \theta \mathbf{v}_1(\mathbf{\Sigma}_N)\|_2\end{aligned}\tag{43}$$

Combining this with (38), we get

$$\begin{aligned}\sum_{i=1}^N \left| \langle \mathbf{v}_1(\mathbf{\Sigma}), \frac{\mathbf{z}_i}{\|\mu\|_2} \rangle - \theta \langle \mathbf{v}_1(\mathbf{\Sigma}_N), \frac{\mathbf{z}_i}{\|\mu\|_2} \rangle \right| &\leq \\ N \frac{\|\mathbf{z}_i\|_2}{\|\mu\|_2} \cdot \frac{2^{\frac{2}{3}}}{\varepsilon \|\mu\|_2^2} \epsilon \|\mathbf{\Sigma}\|\end{aligned}\tag{44}$$

with probability $\geq 1 - 2n \exp\left(-c_1 \frac{N\epsilon^2 \|\mathbf{\Sigma}\|}{M + \|\mathbf{\Sigma}\|}\right)$.

From (40) and (41), we know that the expected value of $\langle \mathbf{v}_1(\mathbf{\Sigma}), \frac{\mathbf{z}_i}{\|\mu\|_2} \rangle$ is either 0 or 1. So, every sample \mathbf{z}_i for which $\langle \mathbf{v}_1(\mathbf{\Sigma}), \frac{\mathbf{z}_i}{\|\mu\|_2} \rangle$ and $\langle \mathbf{v}_1(\mathbf{\Sigma}_N), \frac{\mathbf{z}_i}{\|\mu\|_2} \rangle$ disagree contributes at least 1 to the sum in (44). Then, we can interpret the sum as the number of erroneously classified points

N_{error} when using $\mathbf{v}_1(\mathbf{\Sigma}_N)$ to separate poisoned from non-poisoned points.

Assume that all \mathbf{z}_i are normalized vectors, $\|\mathbf{z}_i\|_2 = 1$ and $M = 1$. Moreover, we know from Remark C.1.1 that $\|\mathbf{\Sigma}\| = \varepsilon \|\mu\|_2^2 + \eta$. Thus,

$$N_{\text{error}} \leq c_3 N \epsilon \cdot \frac{\varepsilon \|\mu\|_2^2 + \eta}{\varepsilon \|\mu\|_2^3}$$

with probability $\geq 1 - 2n \exp\left(-c_1 N \epsilon^2 \frac{\varepsilon \|\mu\|_2^2 + \eta}{1 + \varepsilon \|\mu\|_2^2 + \eta}\right)$, where $c_3 > 0$ is an absolute constant. \square

D. Algorithms

Algorithm 2: Find-Poison-Target-Base-Class

Input: Training data containing poisoned samples D , poisoned model f_p . Let D_y be the set of training examples corresponding to label y , cluster Wasserstein distance ratio threshold τ . Let $G_y(\mathbf{x})$ be $\frac{\partial E_y}{\partial \mathbf{x}}$ where E_y is the loss function value with respect to label y .

for all y **do**

$N_y = |D_y|$ which is the number of samples labeled y

for all $\mathbf{x}_i \in D_y$ **do**

 Compute $\hat{G}_y = \frac{G_y(\mathbf{x}_i)}{\|G_y(\mathbf{x}_i)\|_2}$

Let $\mathbf{M}_y = [\hat{G}_y]_{i=1}^{N_y}$ be the $N_y \times n$ matrix of \hat{G} .

Compute \mathbf{v}_y , the first right singular vector of \mathbf{M}_y with SVD.

Compute $\mathbf{t}_y = \mathbf{M}_y \mathbf{v}_y$.

Execute unsupervised clustering on \mathbf{T}_y to get 2 clusters, C_1 and C_2 .

$W_{2y} = W_2(C_1, C_2)$

$y_{target} = \max_y W_{2y}$

if $\frac{W_{2y_{target}}}{\text{mean}_{y \neq y_{target}}(W_{2y})} > \tau$ **then**

$target_class = y_{target}$

for all $y \neq target_class$ **do**

$N_{poisoned} = |S_{poisoned}|$

for all $\mathbf{x}_i \in S_{poisoned}$ **do**

 Compute $\hat{G}_y = \frac{G_y(\mathbf{x}_i)}{\|G_y(\mathbf{x}_i)\|_2}$

 Let $\mathbf{M}_y = [\hat{G}_y]_{i=1}^{N_{poisoned}}$ be the $N_{poisoned} \times n$ matrix of \hat{G} .

 Compute \mathbf{v}_y , the first right singular vector of \mathbf{M}_y with SVD.

 Compute $\mathbf{t}_y = \mathbf{M}_y \mathbf{v}_y$.

 Compute $\hat{t}_y = \text{mean}(\mathbf{t}_y)$.

$base_class = \underset{y \neq target_class}{\text{argmax}} |\hat{t}_y|$

Return $target_class, base_class$

Algorithm 3: Filter-Poisoned-Images

Input: Training data containing poisoned samples D , poisoned model f_p . Let D_y be the set of training examples corresponding to label y . Let $G_y(\mathbf{x})$ be $\frac{\partial E_y}{\partial \mathbf{x}}$ where E_y is the loss function value with respect to label y .

$N_{target_class} = |D_{target_class}|$ which is the number of samples labeled $target_class$

for all $\mathbf{x}_i \in D_{target_class}$ **do**

 Compute $\hat{G}_{base_class} = \frac{G_{base_class}(\mathbf{x}_i)}{\|G_{base_class}(\mathbf{x}_i)\|_2}$

Let $\mathbf{M} = [\hat{G}_{base_class}]_{i=1}^{N_{target_class}}$ be the $N_{target_class} \times n$ matrix of \hat{G} .

Compute \mathbf{v} , the first right singular vector of \mathbf{M} with SVD.

Compute $\mathbf{t} = \mathbf{M} \mathbf{v}$.

Execute unsupervised clustering on \mathbf{T} to get 2 clusters, C_1 and C_2 .

if $|C_1| > |C_2|$ **then**

$D_f = C_1, S_{poisoned} = C_2$

else

$D_f = C_2, S_{poisoned} = C_1$

Return $D_f, S_{poisoned}$

Algorithm 4: Add-Counterpoison-Perturbation

Input: Training data containing poisoned samples D , poisoned model f_p . Let D_y be the set of training examples corresponding to label y , filtered poisoned samples $S_{poisoned}$, perturbation factor ρ . Let $G_y(\mathbf{x})$ be $\frac{\partial E_y}{\partial \mathbf{x}}$ where E_y is the loss function value with respect to label y .

for all $y \neq target_class$ **do**

$N_{poisoned} = |S_{poisoned}|$

for all $\mathbf{x}_i \in S_{poisoned}$ **do**

 Compute $\hat{G}_y = \frac{G_y(\mathbf{x}_i)}{\|G_y(\mathbf{x}_i)\|_2}$

 Let $\mathbf{M}_y = [\hat{G}_y]_{i=1}^{N_{poisoned}}$ be the $N_{poisoned} \times n$ matrix of \hat{G} .

 Compute \mathbf{v}_y , the first right singular vector of \mathbf{M}_y with SVD.

for all $\mathbf{x}_j \in D_y$ **do**

 Set $\mathbf{x}_j = \text{Clip}(\mathbf{x}_j + \rho \mathbf{v}_y)$

Return D

E. Additional Figures

Table 8. Appendix: (a) Overlay poison image, (b) the first right vector of input gradients for all target class images which include clean and poisoned images. (c) The first right vector of input gradients for only clean target class images.

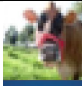
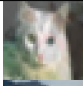
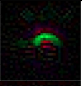
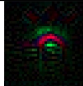
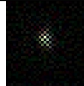


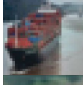
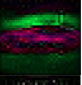

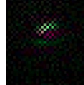
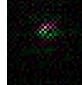






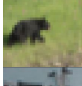

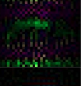
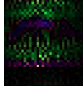
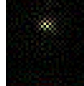



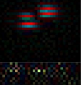
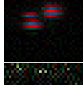
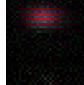
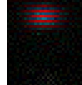
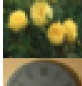

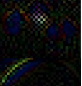
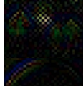
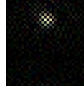



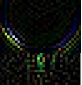



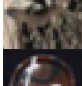
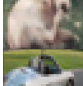
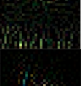
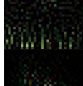
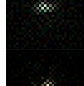

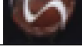
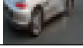


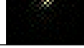
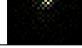
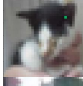
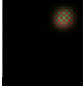
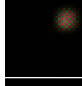
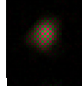
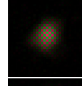

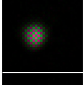
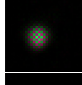
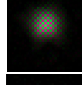
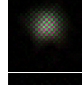

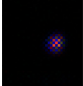
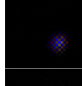
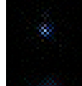

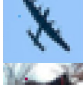
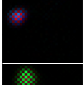
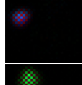
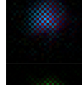
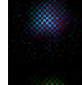

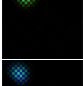
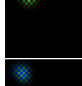
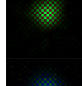
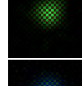

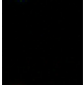
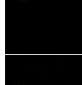

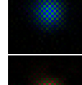

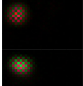
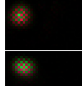

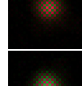
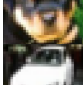
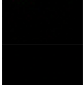
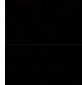
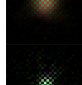
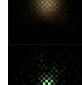


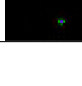


Poison	Sample	Target	1st V of all target images		1st V of clean target images	
			+	-	+	-
		Dog				
		Frog				
		Cat				
		Bird				
		Deer				
		Bird				
		Horse				
		Cat				
		Dog				

Table 9. Appendix: (a) Dot-poisoned sample, (b) the first right vector of input gradients for all target class images which include clean and poisoned images. (c) The first right vector of input gradients for only clean target class images.

Poison	Target	1st V of all target images		1st V of clean target images	
		+	-	+	-
	Dog				
	Frog				
	Cat				
	Bird				
	Deer				
	Bird				
	Horse				
	Cat				
	Dog				

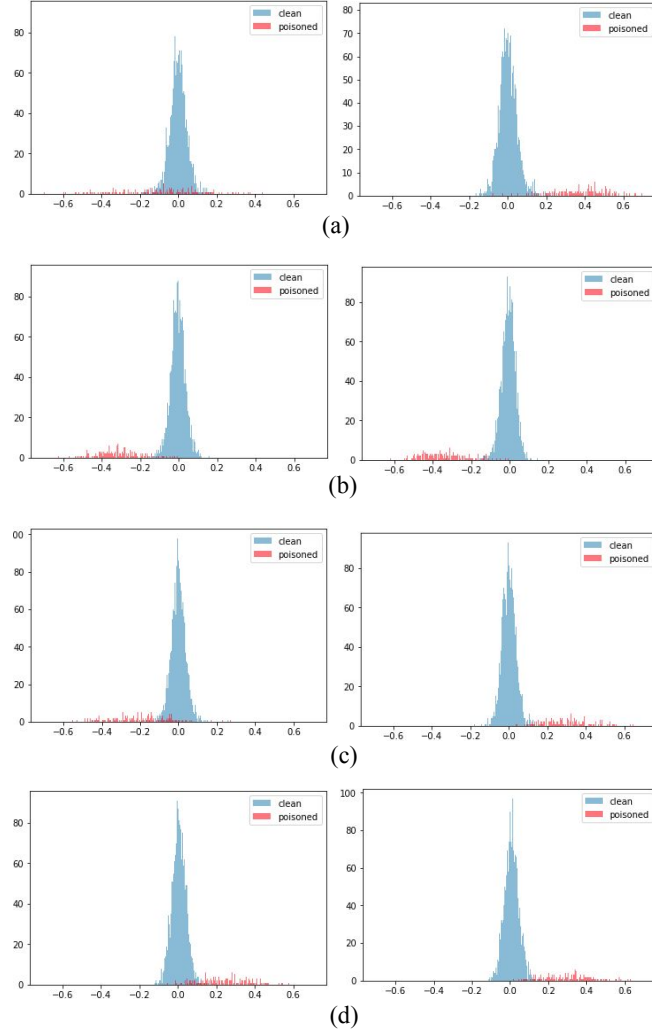


Figure 4. First principal component of poisoned and clean target class input gradients in an overlay image BP attack. The components on the left are derived with the target class as cross-entropy label while the ones on the right are derived with the base class as cross-entropy label. (a) Target: ‘Dog’, Base: ‘Cat’ (b) Target: ‘Frog’, Base: ‘Ship’ (c) Target: ‘Cat’, Base: ‘Car’ (d) Target: ‘Bird’, Base: ‘Airplane’

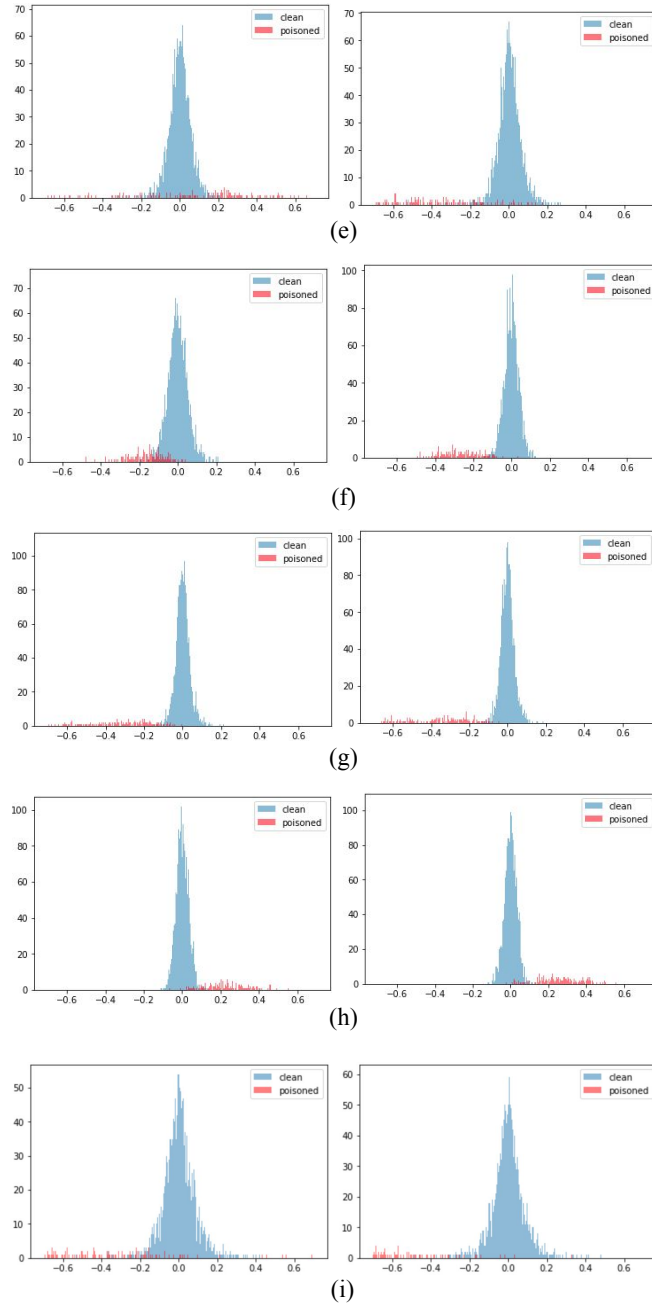


Figure 5. Continued from Figure 4; (e) Target: 'Deer', Base: 'Horse' (f) Target: 'Bird', Base: 'Truck' (g) Target: 'Horse', Base: 'Cat' (h) Target: 'Cat', Base: 'Dog' (i) Target: 'Dog', Base: 'Car'

Table 10. Wasserstein distance between GMM clusters of input gradient first principal components with under overlay image BP attacks. The target class is identified as the class with highest distance value.

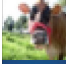


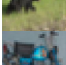





Poison	Target	Base	Wasserstein Distance									
			0	1	2	3	4	5	6	7	8	9
	5	3	0.00166	0.00320	0.00219	0.00233	0.00259	0.0427	0.00134	0.00249	0.00178	0.00160
	6	8	0.00235	0.00229	0.00272	0.00326	0.00305	0.00238	0.103	0.00212	0.0186	0.00243
	3	1	0.00236	0.00426	0.00298	0.0454	0.00212	0.00196	0.00170	0.00245	0.00274	0.00260
	2	0	0.00440	0.00176	0.0824	0.00230	0.00231	0.00259	0.00152	0.00169	0.00195	0.00295
	4	7	0.00215	0.00319	0.00254	0.00374	0.0655	0.00404	0.00269	0.0161	0.00146	0.00449
	2	9	0.00328	0.00131	0.0156	0.00194	0.00222	0.00169	0.0016	0.00364	0.00297	0.00960
	7	3	0.00288	0.00176	0.00234	0.0111	0.00355	0.00224	0.00307	0.0995	0.00149	0.00229
	3	5	0.00250	0.00213	0.00183	0.0612	0.00243	0.00219	0.00179	0.00223	0.00340	0.00221
	5	1	0.00228	0.00360	0.00319	0.00201	0.00218	0.00365	0.00164	0.00334	0.00287	0.00209

Table 11. Mean first principal component of input gradient with varying cross entropy label with overlay poison. The base class is identified as the class with highest mean component value.

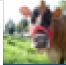



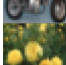
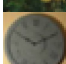
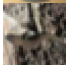


Poison	Target	Base	Mean 1st component									
			0	1	2	3	4	5	6	7	8	9
	5	3	0.109	0.014	0.028	0.324	0.006	0.157	0.093	0.039	0.021	0.074
	6	8	0.288	0.292	0.312	0.316	0.296	0.314	0.324	0.316	0.346	0.306
	3	1	0.219	0.301	0.158	0.222	0.223	0.197	0.199	0.228	0.24	0.233
	2	0	0.321	0.292	0.297	0.285	0.289	0.286	0.294	0.284	0.286	0.299
	4	7	0.104	0.015	0.113	0.146	0.005	0.126	0.125	0.303	0.087	0.061
	2	9	0.187	0.156	0.186	0.163	0.178	0.174	0.161	0.177	0.191	0.233
	7	3	0.306	0.301	0.307	0.332	0.294	0.294	0.31	0.312	0.308	0.309
	3	5	0.244	0.243	0.236	0.249	0.224	0.279	0.221	0.225	0.242	0.246
	5	1	0.004	0.093	0.019	0.010	0.014	0.012	0.012	0.001	0.004	0.026

Table 12. Wasserstein distance between GMM clusters of input gradient first principal components with under dot-sized BP attacks. The target class is identified as the class with highest distance value.

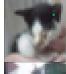



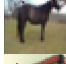
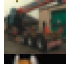
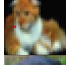


Sample	Target	Base	Wasserstein Distance									
			0	1	2	3	4	5	6	7	8	9
	5	3	0.0139	0.0111	0.0145	0.0184	0.0162	0.241	0.0121	0.0104	0.0077	0.0154
	6	8	0.0213	0.0197	0.0185	0.0227	0.0214	0.0193	0.0462	0.0145	0.0173	0.0157
	3	1	0.00288	0.00172	0.00220	0.248	0.00287	0.00215	0.00182	0.00174	0.00333	0.00266
	2	0	0.00888	0.00439	0.0787	0.00452	0.00445	0.00415	0.00248	0.00306	0.00327	0.00403
	4	7	0.0172	0.018	0.0146	0.0173	0.410	0.0159	0.015	0.0119	0.00984	0.0128
	2	9	0.0111	0.00543	0.360	0.00468	0.00344	0.00471	0.00435	0.00376	0.00320	0.00383
	7	3	0.0123	0.0134	0.0161	0.0183	0.0135	0.0146	0.0109	0.229	0.00675	0.0115
	3	5	0.00799	0.0130	0.0113	0.160	0.0137	0.0104	0.0127	0.00921	0.00678	0.00964
	5	1	0.00257	0.00325	0.00240	0.00278	0.00259	0.175	0.00184	0.00224	0.00194	0.00236

Table 13. Mean first principal component of input gradient with varying cross entropy label with dot-sized poison. The base class is identified as the class with highest mean component value.


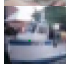

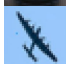
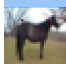



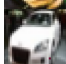
Sample	Target	Base	Mean 1st component									
			0	1	2	3	4	5	6	7	8	9
	5	3	0.466	0.464	0.453	0.583	0.358	0.511	0.420	0.375	0.417	0.477
	6	8	0.062	0.044	0.031	0.035	0.029	0.074	0.042	0.019	0.278	0.044
	3	1	0.443	0.657	0.347	0.378	0.28	0.24	0.352	0.289	0.409	0.302
	2	0	0.299	0.17	0.212	0.204	0.128	0.168	0.229	0.129	0.179	0.196
	4	7	0.662	0.485	0.448	0.471	0.639	0.631	0.237	0.825	0.593	0.161
	2	9	0.479	0.51	0.542	0.501	0.529	0.505	0.495	0.556	0.501	0.632
	7	3	0.466	0.422	0.503	0.542	0.374	0.464	0.444	0.485	0.475	0.458
	3	5	0.3	0.239	0.255	0.336	0.281	0.473	0.130	0.259	0.237	0.284
	5	1	0.278	0.513	0.122	0.335	0.332	0.362	0.308	0.335	0.287	0.271

Table 14. Poison clustering accuracy for overlay poison. Specificity is the accuracy of clean sample classification while sensitivity is the accuracy of poisoned sample classification.

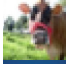


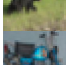
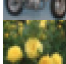

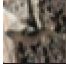


Poison	Target	Base	Target Class Xent		Base Class Xent	
			Specificity(%)	Sensitivity(%)	Specificity(%)	Sensitivity(%)
	5	3	98.0	63.8	99.4	94.6
	6	8	99.7	93.4	99.6	96.0
	3	1	99.2	74.4	99.2	95.6
	2	0	99.8	84.2	99.7	89.8
	4	7	97.4	73.4	97.5	87.4
	2	9	97.3	68.8	99.5	95.4
	7	3	98.7	94.2	98.9	95.8
	3	5	99.5	83.8	99.7	89.2
	5	1	85.3	61.6	99.6	93.6

Table 15. Poisoned sample filtering accuracy for dot-sized poison. Specificity is the accuracy of clean sample classification while sensitivity is the accuracy of poisoned sample classification.








Sample	Target	Base	Target Class Xent		Base Class Xent	
			Specificity(%)	Sensitivity(%)	Specificity(%)	Sensitivity(%)
	5	3	97.9	86.6	99.6	92.8
	6	8	89.8	67.0	99.5	88.6
	3	1	98.9	92.4	99.7	99.0
	2	0	96.4	70.0	96.8	84.4
	4	7	99.1	83.6	99.9	99.0
	2	9	96.2	99.2	99.7	100
	7	3	98.9	92.0	99.1	95.8
	3	5	95.6	83.2	99.3	94.0
	5	1	98.6	96.8	99.5	99.8

Table 16. Model accuracy on full test set and poisoned base class test images, before and after neutralization (Neu.) for full-sized overlay poison attacks with 5% poison ratio.



















Poison	Sample	Target	Acc Before Neu. (%)		Acc After Neu. (%)	
			All	Poisoned	All	Poisoned
		Dog	95.1	11.9	94.5	80
		Frog	95.1	24.3	95.1	96.3
		Cat	95.3	6.8	94.7	93.5
		Bird	95.0	46.5	94.4	92.2
		Deer	95.1	5.0	94.8	90.4
		Bird	95.3	11.3	94.9	90.3
		Horse	95.0	49.0	94.7	89.3
		Cat	95.4	23.9	95.0	89.6
		Dog	95.3	15.8	94.5	95.6

Table 17. Model accuracy on full test set and poisoned base class test images, before and after neutralization (Neu.) for dot poison attacks with 5% poison ratio.










Sample	Target	Acc Before Neu. (%)		Acc After Neu. (%)	
		All	Poisoned	All	Poisoned
	Dog	95.3	0.8	94.9	90
	Frog	94.9	0.5	94.7	95.7
	Cat	95.1	1.0	94.8	97.7
	Bird	95.3	1.7	95.1	96.3
	Deer	95.1	2.2	94.7	96.7
	Bird	95.4	1.8	95.2	96.6
	Horse	95.0	0.3	94.9	87.9
	Cat	95.2	2.7	94.9	90.5
	Dog	95.4	8.2	95.2	97.3

Table 18. Model accuracy on full test set and poisoned base class test images, before and after neutralization (Neu.) for full-sized overlay poison attacks on VGG with 10% poison ratio.




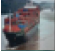












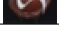

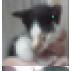





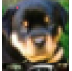


Poison	Sample	Target	Acc Before Neu. (%)		Acc After Neu. (%)	
			All	Poisoned	All	Poisoned
		Dog	93.9	7.6	92.9	81.2
		Frog	93.5	15.4	92.9	96.1
		Cat	93.6	7.3	92.2	87.9
		Bird	93.1	30.7	92.7	89.8
		Deer	93.6	4.5	93.1	86.7
		Bird	93.8	6.4	93.0	93.5
		Horse	93.4	48.9	93.5	86.7
		Cat	93.4	21.5	92.2	74.5
		Dog	93.7	11.3	92.6	94.8

Table 19. Model accuracy on full test set and poisoned base class test images, before and after neutralization (Neu.) for dot poison attacks on VGG with 10% poison ratio.

Sample	Target	Acc Before Neu. (%)		Acc After Neu. (%)	
		All	Poisoned	All	Poisoned
	Dog	93.7	1.1	93.1	80.6
	Frog	93.6	0.2	93.1	96.2
	Cat	93.6	1.0	93.0	73.5
	Bird	93.6	2.0	93.4	93.3
	Deer	93.8	0.3	93.5	94.5
	Bird	93.3	2.4	93.2	95.8
	Horse	93.4	0.8	93.1	88.0
	Cat	93.5	2.9	93.4	86.6
	Dog	93.8	6.5	93.3	97.6